

ABSTRACT

The Influence of Vapor Pressure on Droplet Contact Dynamics on Smooth Surfaces

Austin M. Taylor, M.S.M.E.

Chairperson: Min Y. Pack, Ph.D.

Droplet impact experiments were performed with different fluids using Total Internal Reflection Microscopy (TIRM) on a smooth surface to gain insight into the mechanism for the air film failure of volatile liquids. Several parameters were varied including the impact velocity and droplet volatilities to understand the relationship between the fluid properties and the air film rupture. It was observed that while increasing the Weber number of the impacting droplets generally lead to sooner air film failure, there was significant variance in the magnitude of the contact times at the same Weber numbers for different fluids. It is hypothesized that the vapor output from the droplets themselves, in the immediate area surrounding the droplet, impacts the air film dynamics, as this vapor is constituted by the fluid and thus a different composition compared with the bulk gas in the environment.

The Influence of Vapor Pressure on Droplet Contact Dynamics on Smooth Surfaces

by

Austin M. Taylor, B.S.M.E.

A Thesis

Approved by the Department of Mechanical Engineering

Paul I. Ro, Ph.D., Chairperson

Submitted to the Graduate Faculty of
Baylor University in Partial Fulfillment of the
Requirements for the Degree of
Master of Science in Mechanical Engineering

Approved by the Thesis Committee

Min Y. Pack, Ph.D., Chairperson

Yue Ling, Ph.D.

Seunghyun Kim, Ph.D.

Accepted by the Graduate School
August 2021

J. Larry Lyon, Ph.D., Dean

Copyright © 2021 by Austin M. Taylor

All rights reserved

TABLE OF CONTENTS

LIST OF FIGURES	vi
LIST OF TABLES.....	ix
ACKNOWLEDGMENTS	x
CHAPTER ONE	1
Introduction.....	1
<i>Background</i>	1
<i>Phenomenological Overview of Air Entrainment</i>	4
<i>Pre-Contact Dynamics of the Air Film</i>	9
<i>Air Film Failure and Contact Dynamics</i>	12
CHAPTER TWO	18
Experimental Setup.....	18
<i>TIRM</i>	20
CHAPTER THREE	23
Methodology	23
<i>Experimental Procedure</i>	23
<i>Fluid Properties</i>	27
<i>Drop Size Validation</i>	29
CHAPTER FOUR.....	32
Results and Analysis	32
<i>Pre-Contact Analysis</i>	32
<i>Contact Visualization</i>	38
<i>Data Quality</i>	44
<i>Initial Contact Time</i>	47
<i>Number of Contact Locations</i>	55
<i>Full Contact Time</i>	58
<i>Contact Collapse Time</i>	62
CHAPTER FIVE	66
Conclusions.....	66
<i>Future Work</i>	67
APPENDIX A	69
MATLAB Codes.....	69
<i>TIRM Validation Code</i>	69
<i>Drop Size Code</i>	90

<i>Background Subtraction Code</i>	98
BIBLIOGRAPHY	103

LIST OF FIGURES

Figure 1.1 Standard droplet impact model.....	2
Figure 1.2 First droplet impact observations	3
Figure 1.3 Depiction of categories of droplet impact responses on a solid substrate	3
Figure 1.4 Entrapped air bubble in experiments	5
Figure 1.5 n-Heptane and molten nickel droplets with entrapped air bubbles	6
Figure 1.6 Impact to entrapped bubble progression concepts [10, 11] and visualization [12].....	7
Figure 1.7 Air bubble in “air disk”	8
Figure 1.8 TIR droplet impact image sequence	9
Figure 1.9 Air film morphological progression	10
Figure 1.10 Air film profiles during droplet spreading and recession	10
Figure 1.11 We number effect on air film profile.....	11
Figure 1.12 Standard air film analysis diagram with magnified air entrainment area.....	12
Figure 1.13 Air film tracking with color interferometry.....	14
Figure 1.14 Air film profile leading to contact	14
Figure 1.15 Viscous oil droplet with several contact points	15
Figure 1.16 Effect of droplet viscosity on air film profile.....	15
Figure 1.17 Toroidal ring of contact sites.....	16
Figure 2.1 Experimental apparatus overview	18
Figure 2.2 Optical apparatus overview	19
Figure 2.3 Custom prism holder	20
Figure 2.4 What TIRM captures	22

Figure 3.1 Raw drop size images: mixture 1	30
Figure 3.2 Droplet diameter measurements	31
Figure 4.1 Pre-contact water reflectance vs normalized radius	33
Figure 4.2 Pre-contact ethanol reflectance vs normalized radius	33
Figure 4.3 Pre-contact mixture 2 reflectance vs normalized radius.....	34
Figure 4.4 Pre-contact mixture 1 reflectance vs normalized radius.....	34
Figure 4.5 Pre-contact acetone reflectance vs normalized radius.....	35
Figure 4.6 Pre-contact water normalized air film height vs normalized radius.....	35
Figure 4.7 Pre-contact ethanol normalized air film height vs normalized radius	36
Figure 4.8 Pre-contact mixture 2 normalized air film height vs normalized radius	36
Figure 4.9 Pre-contact mixture 1 normalized air film height vs normalized radius	37
Figure 4.10 Pre-contact acetone normalized air film height vs normalized radius	37
Figure 4.11 Finding contact frame.....	39
Figure 4.12 Typical water contact	41
Figure 4.13 Typical acetone contact	41
Figure 4.14 Typical ethanol contact.....	42
Figure 4.15 Typical mixture 1 contact.....	42
Figure 4.16 Typical mixture 2 contact.....	43
Figure 4.17 Contact routes on contaminated surfaces	45
Figure 4.18 Potential visual obscurities	46
Figure 4.19 Typical video backgrounds.....	47
Figure 4.20 Initial contact time definition	48
Figure 4.21 Initial water contact	49
Figure 4.22 Initial acetone contact.....	49
Figure 4.23 Initial ethanol contact	50

Figure 4.24 Initial mixture 1 contact.....	50
Figure 4.25 Initial mixture 2 contact.....	51
Figure 4.26 Weber number vs initial contact time.....	52
Figure 4.27 Weber number vs nondimensional initial contact time	53
Figure 4.28 Vapor pressure vs initial contact time	53
Figure 4.29 Vapor pressure vs nondimensional initial contact time.....	54
Figure 4.30 Typical contact progression for acetone droplets.....	55
Figure 4.31 Number of contact points vs Weber number	56
Figure 4.32 Number of contact points vs vapor pressure	57
Figure 4.33 Full contact identification.....	58
Figure 4.34 Weber number vs full contact time	59
Figure 4.35 Weber number vs nondimensional full contact time	59
Figure 4.36 Vapor pressure vs full contact time	60
Figure 4.37 Vapor pressure vs nondimensional full contact time	60
Figure 4.38 Number of contact points versus dimensionless full contact time	62
Figure 4.39 Contact collapse time versus Weber number	63
Figure 4.40 Dimensionless contact collapse time versus Weber number.....	63
Figure 4.41 Contact collapse time versus vapor pressure.....	64
Figure 4.42 Dimensionless contact collapse time versus vapor pressure	64
Figure 4.43 Number of contact points versus dimensionless contact collapse time.....	65

LIST OF TABLES

Table 3.1 Droplet Fluid Properties.....	29
Table 3.2 Droplet Diameter Summary.....	31
Table 4.1 Release Height to Weber Number	40
Table 4.2 Summary of Experiments with Contact.....	40

ACKNOWLEDGMENTS

I would like to thank the Baylor Mechanical Engineering Department for allowing me to conduct this research and use the wonderful laboratory resources of the BRIC. I also am very grateful for Dr. Wright, Dr. Ling, and Dr. Rylander for writing my recommendations and answering any questions I had about graduate school while I was considering applying.

I am grateful to Dr. Min Y. Pack for allowing me to be a part of his lab. Without Dr. Pack, I would have never thought to conduct this research. It was also a pleasure to work with and spend time with the other graduate students, Ziwen He and Huy Tran, in Dr. Pack's lab. I wish all of the lab success in all their future endeavors.

Last but certainly not least, I would like to thank my family and my wife for their constant support throughout this degree program. Progressing through this degree was very difficult, and without their support I likely would not have finished this program.

CHAPTER ONE

Introduction

Background

Liquid droplets affect many areas of life. They are involved in numerous applications ranging from pesticide distribution to internal combustion engines to spray coatings [1]. Depending on the application, the droplets either contact or bounce off the target surface. For example, with pesticide distribution, the goal is to coat the desired vegetation with the pesticide spray and not allow the droplets to run off of the surface of the vegetation and end up in the ground water supply. Understanding the mechanisms behind liquid droplet contact is pivotal to improving these technologies and many more.

Droplet impact research is categorized depending on what the droplet is impacting. The main categories include solid surfaces and bathes of liquid. Some drop impact studies utilize a lubricating oil film to provide a smooth film [2]. Another method for achieving smooth surfaces is to cleave off the top layer of a mica slab, as the microstructure of the material leaves an atomically smooth surface [3, 4]. The solid aspect of the surface is to prevent surface deformation from affecting the droplet impact response, as the geometry of the surface would change. While studies with droplet impacts onto inclined surfaces are useful for various applications, keeping the surface horizontal allows the probing of the fundamental mechanisms of contact more consistently.

The behavior of droplet impacts on solid, lubricated, horizontal surfaces varies drastically depending on several variables. There are kinematic variables, fluid

properties, and environmental factors to consider. Kinematic variables include the impact velocity of the droplet and the diameter of the droplet. The viscosity, surface tension, density, and vapor pressure of the droplet all constitute the fluid properties. The environmental factors encompass the same variables as the fluid properties except they correspond to the fluid that the environment is made from instead of the fluid the droplet is made from. The ambient temperature, pressure, and relative humidity are also environmental factors that affect the results of droplet impacts. Figure 1.1 below is from Liang's paper and is a diagram of the relevant variables to consider in a droplet impact experiment.

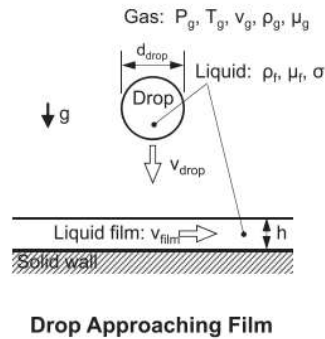


Figure 1.1 Standard droplet impact model [1].

Droplets have been studied for over a hundred years, as their applications are vast and critical to several fields. One of the past researchers to study droplet impacts was A.M. Worthington. The fingering of the sheet of the liquid spreading out from the bottom center of the droplet was one of the main features identified in their research (see Figure 1.2).

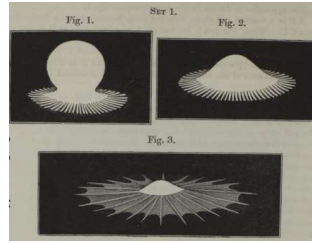


Figure 1.2 First droplet impact observations [5]

As time moved on more studies were conducted. Most pursuits were focused on the geometry or morphology of the droplet throughout the impact process. Information was gathered to determine the overall shape and the micro-features created at the bottom of the droplet, as capturing the shapes of these features is a critical method for gaining understanding of the behavior of the droplet. Researchers have identified multiple responses of droplet impacts as depicted below in figure 1.3.

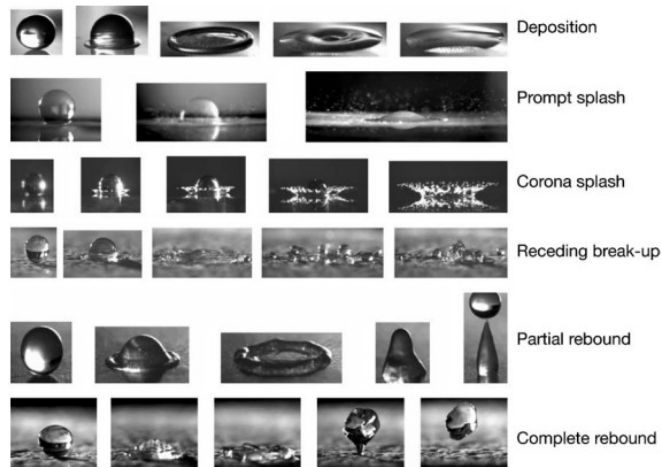


Figure 1.3 Depiction of categories of droplet impact responses on a solid substrate [6].

Grouping variables together to become dimensionless combinations is often useful for classifying research and results more generally. For droplet impact research,

there are several nondimensional numbers. Written below are the ones that most often arise, depending on the focus of the experiment.

$$\begin{aligned} \text{Re} = \frac{\rho V d}{\mu} \quad \text{We} = \frac{\rho V^2 d}{\gamma} \quad \text{Oh} = \frac{\mu}{\sqrt{\rho \gamma d}} = \frac{\sqrt{\text{We}}}{\text{Re}} \quad \text{Bo} = \text{Eo} = \frac{\Delta \rho g d^2}{\gamma} \\ \text{Fr} = \frac{V}{\sqrt{g d}} \quad \text{Ca} = \frac{\mu V}{\gamma} = \frac{\text{We}}{\text{St}} \quad \text{St} = \frac{\mu}{\rho V d} \quad \text{Kn} = \frac{\lambda}{h} \end{aligned}$$

In the above equations, d is the droplet diameter prior to deformation, γ is the surface tension of the droplet, λ is the mean free path of the air (drop impact environment), ρ is the density of the droplet, V is the impact velocity of the droplet, h is the air film thickness, and μ is the droplet viscosity. Some papers will use the radius of the droplet or other relevant length for the length scale. The Reynold's number, Re , compares the inertial and viscous effects. The Weber number, We , compares the inertial and capillary effects. The Ohnesorge number, Oh , compares the viscous to inertial and capillary effects. The Bond, Bo , or Eotvos number, Eo , compares the gravitational to capillary effects. The Froude number, Fr , compares the inertial and gravitation effects. The Capillary number, Ca , compares the viscous and capillary effects. The Stokes number, St , is often defined as the inverse of the Reynold's number for droplets research. The capillary length relates gravity and capillarity to determine a maximum length for that fluid. The Knudsen number, Kn , compares the mean free path to the relevant length scale to determine if the environment should be considered a rarefied gas or not.

Phenomenological Overview of Air Entrainment

The identification of an air bubble entrapped within the droplet after the droplet has made contact with the substrate. Figure 1.4 below is an example of droplet impact research which observed an entrapped air bubble inside the droplet.

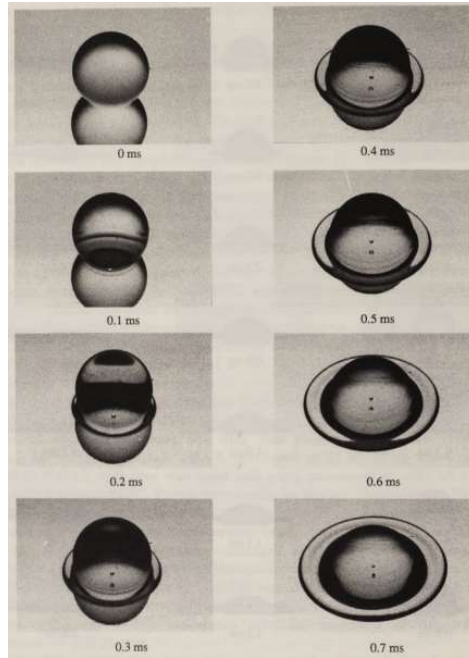


Figure 1.4 Entrapped air bubble in experiments [7].

With figure 1.4 above, the focus was on the Leidenfrost effect (this figure was a control case on an unheated substrate), but this droplet image sequence shows the existence of the entrapped air bubble. This bubble naturally provokes the question of its origin.

Driscoll et al. studied droplets that flatten out into a disk shape upon impact, and still have an entrapped air bubble where the air entrainment over time was tracked as well as the droplet rim velocity when air entrainment stops using interferometry [8, 9]. The Weber number of these impacts varied from around 100 to 1000. Figure 1.5 below shows droplets constituted by other fluids than water still trap an air bubble during impact.

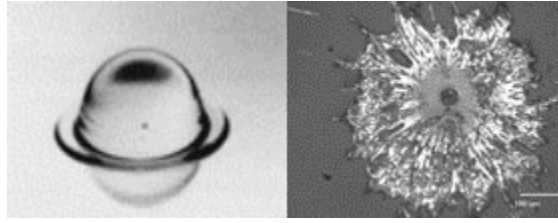


Figure 1.5 n-Heptane and molten nickel droplets with entrapped air bubbles [10]

Mehdi-Nejad et al. [10] showed that even though n-heptane and molten nickel have very different fluid properties than water, they still develop similar air pockets upon impacting with a solid substrate as water droplets. This demonstrates that there was not just a perfect combination of fluid properties with water that formed the dimple, but that the dimple is a common feature to all droplet impacts. Furthermore, the dimple shape and size are shown to vary with the fluid properties as the bubbles in the n-heptane and molten nickel are visibly different diameters.

The next major step in understanding was to figure out why there is only one bubble of air in the droplet and why it always near the middle. Figure 1.6 below depicts different proposed progressions that would produce the single air bubble in the middle of the droplet.

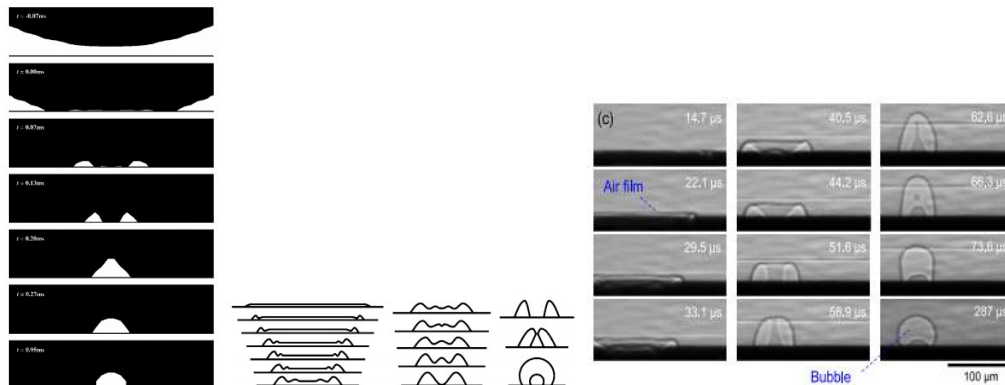


Figure 1.6 Impact to entrapped bubble progression concepts [10, 11] and visualization [12]

Both Mehdi-Nejad et al. [10] and Thoroddsen et al. [11] proposed progressions of the air bubble formation under the droplet. They were based on capillary effects and minimization of surface area. It is asserted that the origin of the air bubbles were perturbations on the bottom edge of the droplet that coalesce into one air bubble under the center of the droplet. Lee et al. [12] used an x-ray imaging technique to observe the trapped air bubble from the side and track its morphological progression. What Lee et al. observed very closely matched the bubble progression put forth by Thoroddsen et al. [11].

Considering the small scale of the air layer under the droplet, rarefied gas conditions can apply along the bottom flattened surface of the droplet nearest the substrate. Duchemin and Josserand [13] studied and attempted to correct equations and considerations for the rarefied gas effect on the air entrainment in droplets. Duchemin and Josserand concluded that the entrapped air bubble size depends on the environmental gas pressure, but Duchemin and Josserand do assume the air layer is much smaller than the mean free path of the environmental gas on average over the air layer.

Measurement techniques also evolved to allow not only side view imaging of droplet impacts, but also bottom views. These bottom views allowed more precision in understanding where and how the droplet contacts the substrate. Thoroddsen used a clear substrate to allow light to pass through it and determine the thickness of the air layer under the droplet using interferometry. Thoroddsen et al.'s research included droplet impacts with Weber numbers ranging from 20 - 1500. Figure 1.7 below shows the air

disk, which is the proposed starting form of the trapped air bubble, during a droplet impact.

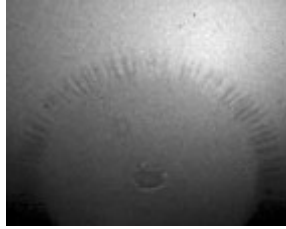


Figure 1.7 Air bubble in “air disk” [11]

Fujimoto et al. [14] used Total Internal Reflection (TIR) to capture the thickness of the air film underneath the droplet from a bottom view as shown in figure 1.8 below. As is evident in the image sequence, there is a bright spot in the middle, indicating an air gap at the stagnation point. This is the origin of the entrapped air bubble visualized by other researchers. These researchers tracked the inner and outer diameters, picked up with this optical technique, over time at various We numbers. The inner diameter starts at its maximum value of nearly half a millimeter, while the external diameter starts at its smallest value and grows larger until it is around 2 millimeters in diameter. Across all the We numbers in this study, the inner diameters of the droplet always decreased to approximately the same value, while their starting values varied directly with the We number.

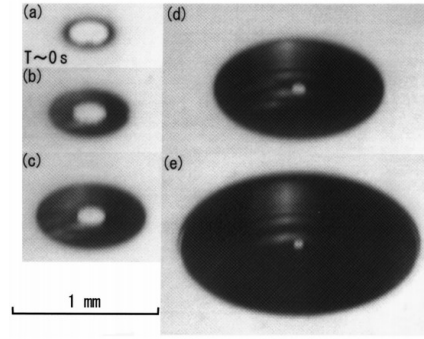


Figure 1.8 TIR droplet impact image sequence [14]

Pre-Contact Dynamics of the Air Film

Now that the “air disk” has been established as what precedes the trapped bubble, the next question is how and why does the air disk form. Researchers have tried to answer this question by measuring the air disk, or air film as it is named today, with different droplet impacts, and characterizing their results using nondimensional numbers and groups. Some researchers prefer to simulate droplet impact experiments and view the corresponding results with the focus being on what occurs in the air film below the droplet.

Mandre et al. [15] simulated a droplet impact and observed the thin air film supporting the droplet. Figure 1.9 below shows the air film profile progression identified in Mandre et al. simulations and the corresponding pressure profile. Mani et al. [16] further investigated the results of droplet impact simulations and mapped the dimple height as a function of the pressure of the environment and separately the impact velocity. Mani et al. developed equations relating the maximum pressure in the air film to the minimum dimple height, impact velocity, and others. Mani et al. also showed that as the ambient pressure is increased the maximum dimple height is decreased.

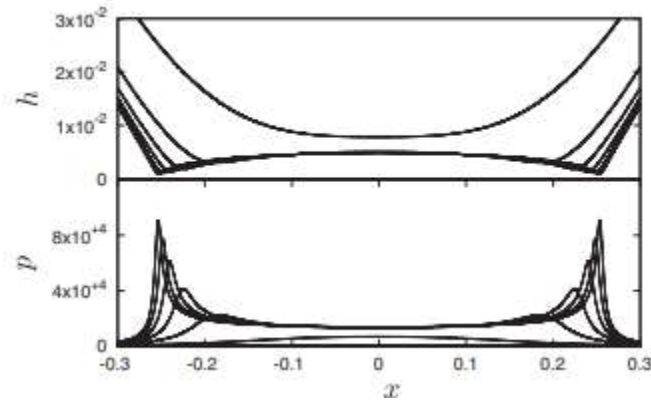


Figure 1.9 Air film morphological progression [15]

de Ruiter et al. and Bouwhuis et al. [17, 18] used interferometry to measure the air film profile in impacting droplets with low We numbers. Figure 1.10 below shows the temporal evolution of the air film profile as the droplet impacts and rebounds, respectively. de Ruiter et al. mapped the wetting, bouncing, and hovering droplet impact response regimes vs We number. Hovering is the regime where the droplet appears to be sitting on the substrate to the naked eye but can still oscillate until it contacts the substrate. Hovering can last for more than a quarter of a second [19]. When the droplet is hovering the whole air film has a thickness less than a micron and is relatively flat or devoid of a dimple [19].

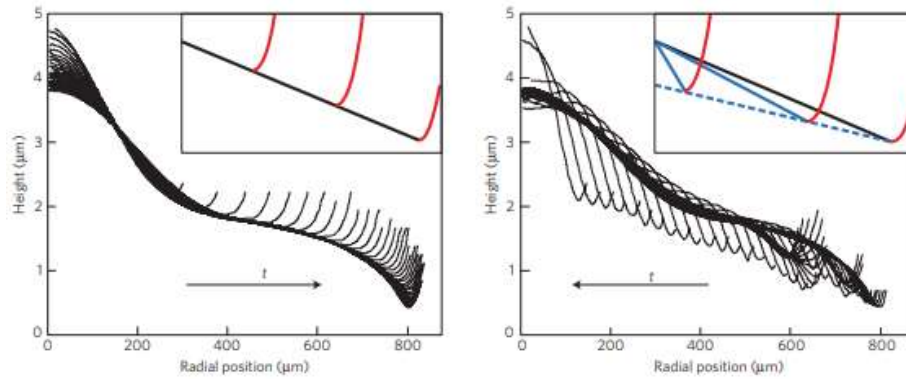


Figure 1.10 Air film profiles during droplet spreading and recession [17]

de Ruiter et al. [20] further tracked the effect of We number on the air film profile, showing how as We number increases the maximum height of the dimple decreases and the radius of the air film profile increases. One of de Ruiter et al.'s figures demonstrating the We number effect on the air film is depicted below in figure 1.11.

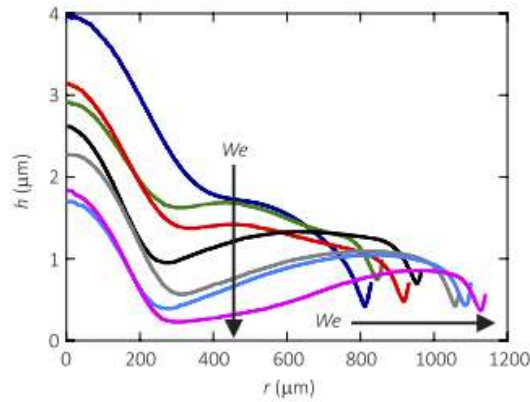


Figure 1.11 We number effect on air film profile [20]

Klaseboer et al. [21] created models for the dimple height as functions of the velocity and separately the capillary number using the data collected by Bouwhuis et al. When plotted on a log-log plot the dimple height is directly proportional to the capillary number. The dimple height is dictated by the capillarity of the droplet at very low impact velocities and by the Weber number at high impact velocities. The maximum dimple height for any droplet occurs at the impact velocity that satisfies equation 1.1 below.

$$We = 1 + Bo \quad (1.1) [21]$$

Kolinski et al. [22] took the TIR optical technique previously utilized for visualization of the droplet underside and calculated the corresponding gap thickness. Kolinski et al. then was able to show the true morphological progression of the bottom

surface of the droplet as it first comes into the spatial view of the TIR technique and then makes full contact. Kolinski et al.'s observations agree well with the morphological progression put forth by Thoroddsen and de Ruiter as described previously. Kolinski later tracked the morphological progression of the air film, specifically the radially values of the minimum air film thickness and edge of the air film [23]. Kolinski et al. has also shown that water droplets can bounce off of perfectly hydrophilic surfaces, although Kolinski et al. states this is more of an exceptional response than a typical response [3].

Air Film Failure and Contact Dynamics

Figure 1.12 below is the typical diagram to demonstrate the key features present to consider for an air film and contact analysis of a droplet impact. There are multiple heights that come into play. There is the dimple which is located in the center of the drop in the region most effected by the stagnation point in the air flow around the droplet. Then the height of the flat region created by the drop momentum and substrate. The air in this region is usually modeled using lubrication theory due to the height of the flat region being around 3 orders of magnitude smaller than the droplet diameter prior to deformation. The radial extent of the flattened bottom region of the droplet is also a relevant metric to track in the air film analysis.

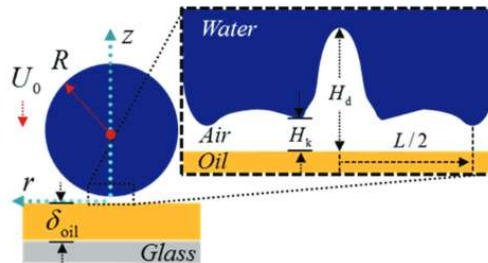


Figure 1.12 Standard air film analysis diagram with magnified air entrainment area [2]

Pack et al. [2] tracked the temporal progression of the air film profile for We numbers of 3.2 and 18 using TIRM. Pack et al. also measured the contact time of the droplet impacts and plotted them versus We number and also versus a combination of several fluid parameters raised to various powers. Pack et al. ultimately concluded that when We number exceeds a value of 10 the disjoining pressure causes the air film to fail at kink, or the first inflection point radially outward from the dimple, and when the We number (with drop radius as the length scale) is between 2 and 10 the capillary wave that propagates through the droplet causes the dimple to collapse and make contact in the middle of the droplet.

Van Der Veen et al. [24] used color interferometry to observe the air film under the droplet as shown in figure 1.13. Van Der Veen et al. tracked the vertical velocity of the center of the dimple and used that to find the corresponding horizontal velocity of the air at the sides of the air film profile. This technique has the advantage of viewing the entire dimple, as the TIR approach cannot view far enough to see the top of dimples in water droplets.

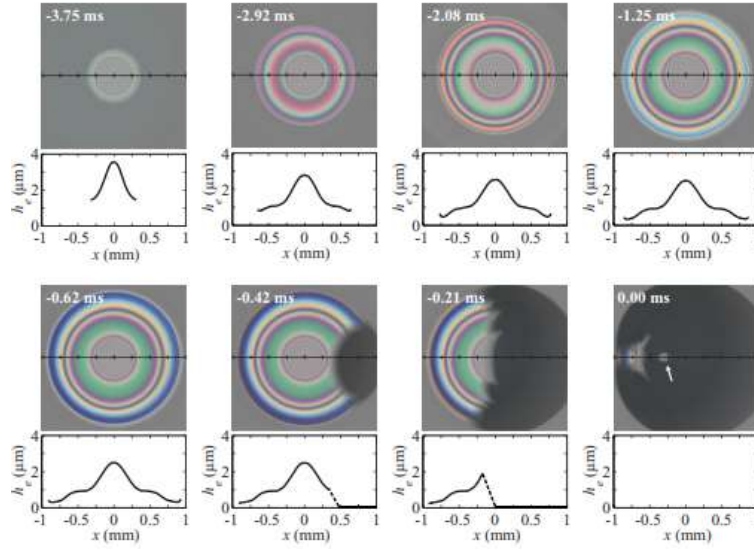


Figure 1.13 Air film tracking with color interferometry [24]

Li and Thoroddsen [25] used interferometry to map the temporal progression of an impacting drop that makes contact before it can recede and start rebounding as shown in figure 1.14. Figure 1.14e depicts the initial formation of the air film as the droplet approaches the substrate, while figure 1.14f shows the air film progression thereafter leading to contact with the substrate.

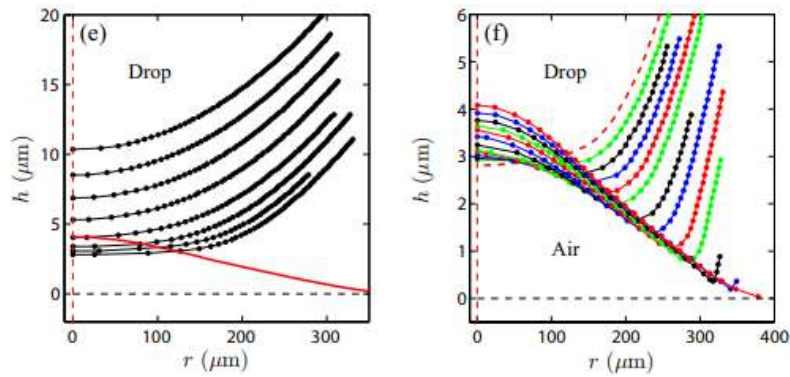


Figure 1.14 Air film profile leading to contact [25]

Langley et al. [26] performed droplet impact experiments using silicone oils of incremental viscosity, ranging from a water, control droplet, to a silicone oil with 20 million centistokes. Langley used color interferometry to measure the air film as depicted below in figure 1.15. There are multiple dark dots present in the droplet visualization, and these represent separate contact initiation points. Langley also tracked the average radial profile of the air film corresponding to each viscosity droplet used and those results are plotted below in figure 1.16. The viscosity of the droplet has a similar relationship to the air film profile as the We number of the impact, with the exception that larger We number impacts not only lower the dimple height but also increase the radial extent of the air film whereas the viscosity of the droplet only effects the dimple height.

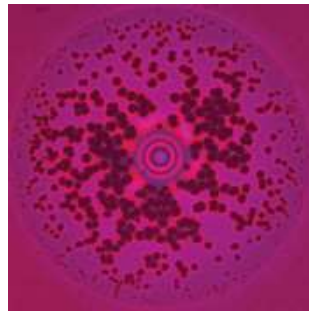


Figure 1.15 Viscous oil droplet with several contact points [26].

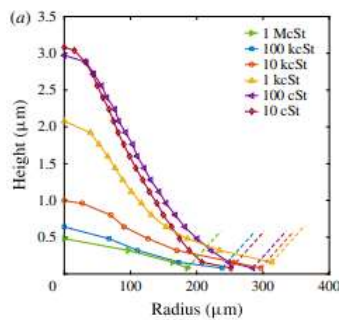


Figure 1.16 Effect of droplet viscosity on air film profile [26].

Li et al. [4] conducted droplet impact experiments on freshly cleaved mica surfaces and found that the double contact ring depicted below in figure 1.17 occurred when the rarefied gas regime was applicable. This bifurcation of the air film was not a result for a specific Weber number impact, but rather for a specific compressibility of the ambient fluid (air) based on the droplet impact velocity and fluid properties of the ambient fluid.

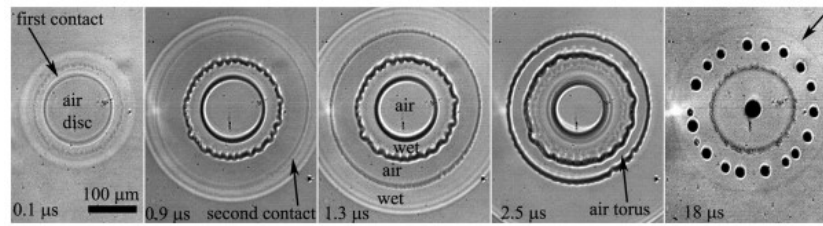


Figure 1.17 Toroidal ring of contact sites [4]

Separately, Li et al. [27] performed droplet impact experiments on solid surfaces with varying surface roughness to gain insight into its effect on the contact dynamics of droplet impacts that result in a thin sheet droplet morphology. Li et al. asserted that the imperfections on the substrate provided locations for the air film to rupture and the droplet to contact the substrate. However, their results only show the final contact patch of the droplet, and how with rougher surfaces the contact patch has bubble laden edges. Their initial contact method was only theorized based on their observations of the final contact patch.

In summary, there is an air film that forms underneath a droplet before it impacts the substrate in its path, and the formation and collapse of the air film are critical to understand and predict the response behavior of the droplet. The We number is one of the most important dimensionless parameters for droplet impact studies, as its magnitude

affects the relative heights of the dimple and flat portion of the air film, as well as potential air film failure mechanisms as identified by Pack et al. However, there are other parameters that become more important than the We number under certain circumstances, as is demonstrated with the bifurcation of the air film under the right ambient environment compressibility by Li et al. Langley et al. demonstrated that the viscosity of the droplet can also become the dominant parameter in a droplet impact and its contact progression. There has not been a study that varied the vapor pressures of the droplets to assess how the vapor pressure could affect the contact mechanisms and air film progression in droplet impacts. The goal of this thesis is to explore the effect of the vapor pressure and fill in this gap of knowledge. For the purposes of this study, only solid, lubricated, horizontal surfaces were used.

CHAPTER TWO

Experimental Setup

The overall experimental apparatus has three main functional groups. An overview of how those groups interact with each other is visualized below in figure 2.1.

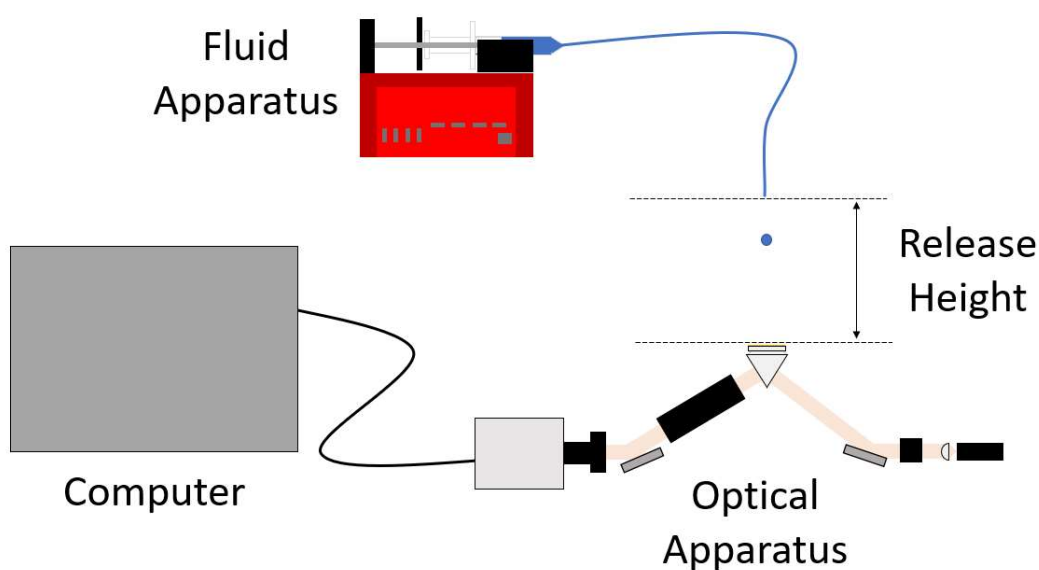


Figure 2.1 Experimental apparatus overview

The fluid apparatus contained a syringe pump, a fluid filled syringe, plastic tubing, luer lock connections, and a 30-gauge needle. The syringe pump controlled the fluid flow through the tubing and ultimately the droplet creation at the tip of the needle. The tubing was cut to sufficient length to remain slack to allow for vertical adjustment of the needle location relative to the substrate surface. The distance between the tip of the needle and the top of the substrate is referred to as the release height, as indicated in figure 2.1. Figure 2.2 below shows a more detailed view of the optical apparatus from

figure 2.1, to illustrate how all the optical components interact with each other. The LED used was Thorlabs M625L4 with a wavelength of 636.23 nm when maximum power output is utilized. The lens right after the LED is an aspheric lens used to collimate the light into a beam. The polarizer allowed the light to be p-polarized as this produces slightly more linear relationships from the TIRM equations. Mirrors were utilized to minimize the horizontal footprint of this apparatus upon the optics table and achieve the desired angle of incidence onto the top of the imaging surface. The mirrors were set to 22.5 degrees to produce an incident angle of 45 degrees onto the top surface of the prism. The oil layer changes this angle to 49.7 degrees. This angle was chosen to be beyond the critical angle needed for total internal reflection between the glass-air and oil-air boundaries respectively, as will be discussed in more detail later. The objective used was a Mitutyoyo 5x lens and the camera used was a Photron NOVA S9.

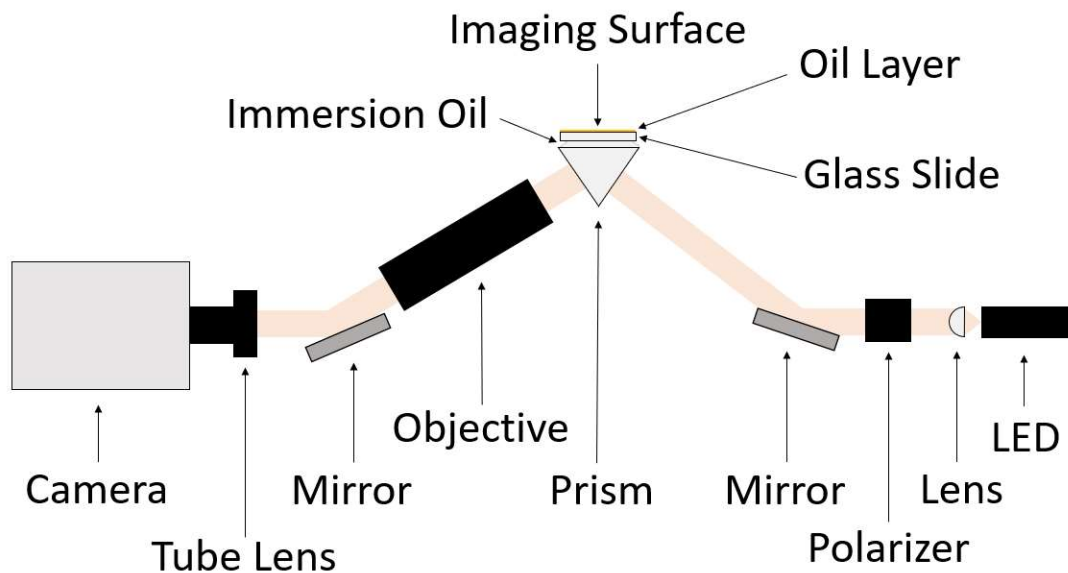


Figure 2.2 Optical apparatus overview

The prism holder depicted in figure 2.3 was designed to constrain the prism properly while still allowing light to both enter and exit the faces of the prism and not impede the placement and movement of the glass slide that is placed on top of the prism.

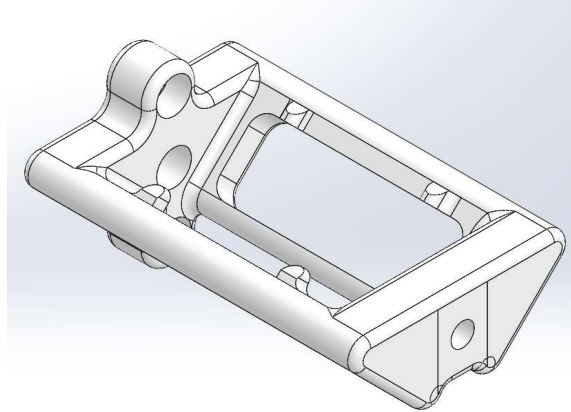


Figure 2.3 Custom prism holder

A key detail with the configuration of this experimental apparatus is the elevation of the prism and use of mirrors to allow the overall apparatus to conserve space horizontally. This elevation changes the incident angle of the light onto the top surface of the prism, which is a key variable in the use of TIRM as will be discussed later.

TIRM

Overview

Total Internal Reflection Microscopy (TIRM) also referred to as Frustrated Total Internal Reflection (FTIR) is an optical measuring technique that leverages a unique property of light rays that are totally internally reflected. Shirota et al. [28] detailed and validated this technique. Despite the light rays appearing to not pass through the boundary of the medium, there is actually an evanescent wave that is generated at this

boundary. The evanescent wave generated from the totally internally reflected light decays over a length of approximately one wavelength of the light source used.

When an object enters the space occupied by the evanescent wave, the light from the evanescent wave will enter the object if the index of refraction is greater than the ambient. This results in the image recorded by the camera becoming correspondingly darker in the affected regions.

Figure 2.4 below is a dramatic visualization of what the TIRM technique is capturing when a droplet is about to impact the substrate. When recording images with TIRM, the resulting image will darken in the regions where a droplet (or another object) is coming close enough to the substrate surface to enter the region observed by the evanescent wave. As the droplet enters the evanescent wave, the light in the evanescent wave can now enter the droplet medium. This results in less intensity of the light reflecting to the camera and instead now travelling through the droplet itself. A detail that can complicate the TIRM image results, is that the light that is now in the droplet could reflect off the droplet-air boundary and end up going back into the prism and ultimately back to the camera. The image has bright spots in these areas. Note that the “dimple” formed at the stagnation point of the droplet, is typically beyond the range of TIRM.

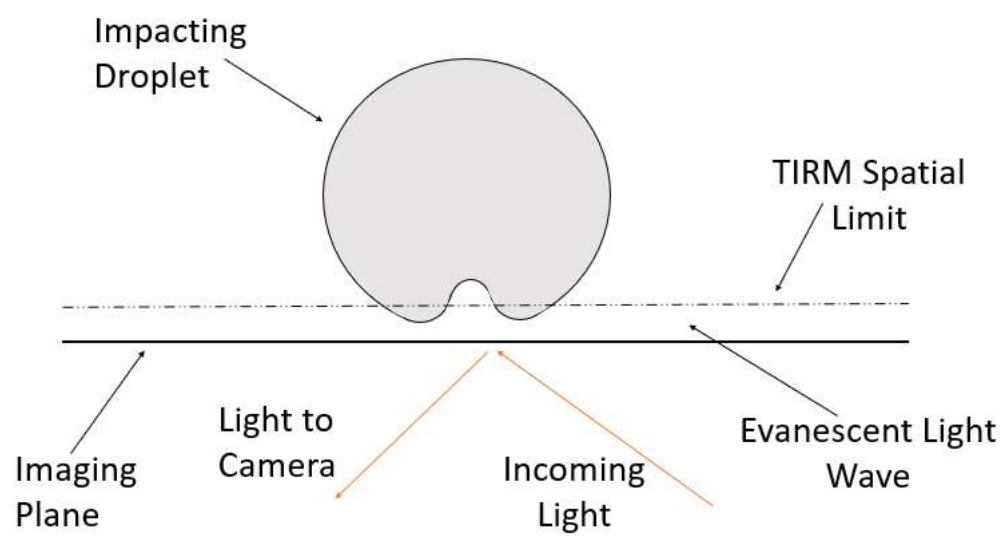


Figure 2.4 What TIRM captures

CHAPTER THREE

Methodology

Experimental Procedure

The essential elements of the experiment are as follows: the droplets must be impacting onto a perfectly smooth surface, the optics must be clean to not impede data in the images, the incident angle of the light source onto the top surface of the prism must allow TIRM to function, the droplets must be released slowly, the release height of the droplets must be measured, and the droplets must be contamination free.

With regard to ensuring a perfectly smooth surface for the droplets to impact onto, an oil layer was applied to glass slides. The glass slides were used for the convenience of moving the slide around on top of the prism to a new, clean area on the slide for a droplet to impact onto. This allows multiple droplet impacts to be recorded between cleanings of the prism or in this case glass slides.

The glass slides were provided by the manufacturer pre-cleaned. Despite that, if the glass slide was used with the spin coater immediately, there were always a few imperfections or specks of dust that inhibited the spin coating process and left visible radial streaks in the oil film. To prevent those streaks from forming, the glass slides were cleaned just as thoroughly as any other optical component, before entering the spin coater.

The spin coater had its own programmed series of rotational velocities and durations to properly spread out the oil layer to the desired thickness. The glass slide

after being cleaned was weighed with a high precision scale to the nearest tenth of a milligram. Then the slide was coated with oil in the spin coater and reweighed in the scale. The difference in the weights before and after oil coating were recorded for each slide used. The oil used to coat the slides was a silicone oil with a viscosity of 1000 cSt. This oil selection and spin coater settings resulted in an average oil film thickness of around 3.7 - 4.0 microns.

The flowrate used to generate the droplets was determined experimentally. This value varied for the different fluids used. Generally, the slowest flowrate possible was used within reason. For more volatile fluids like acetone, the flowrate had to be increased. The acetone would release a lot of vapor to the point where the droplet would never drop with the flowrate used for water for example. Another issue that arose with the use of acetone is the vapor causing some smaller drops to leak out of the needle when undesired. Fortunately, this extra leakage was not fast enough to ruin any good data captured, it was just inconvenient as the space on the glass slide would get used up by these extra drips.

Measuring the release height of the droplet is critical to proper data analysis. The release height is one of the variables used in calculating the Weber number. The Weber number assesses the balance between the inertial and surface tension forces. It is typically used in the droplet impact community to categorize the impact. The Weber number can help predict whether the droplet will splash or just bounce upon impact for example. The release height refers to the distance between the end of the needle used to generate the droplet and the top surface of the oil film on the glass slide for these experiments. The release height was measured using a ruler attached to the vertical shaft

that the needle was sliding along. The release height was calibrated for each experimental session to be safe. The calibration process was straight forward. The needle was lowered until it was just barely contacting the oil film layer. The ruler was then adjusted to align the 1 cm mark with the bottom edge of the needle adjusting linkage. It was aligned with the 1 cm mark just to ensure the actual markings on the ruler were used and not the overall length of the ruler itself. The needle assembly was then raised up to in increments of 0.5 cm for the varying droplet release heights. The heights ranged from 0.5 cm to 4.0 cm in increments of 0.5 cm. These distances were selected based on the corresponding Weber number of room temperature water released from these heights. Water's characteristics for droplet impact were already studied, and this range of release heights gave a corresponding range of Weber numbers from 2.9 to 23.2. These Weber numbers encompass bouncing droplet impacts to immediate air film collapse droplets, which is the relevant range of dynamic responses of interest for this experiment. All the other fluids were released from these same heights for experimental consistency. This led to the other fluids having different ranges of Weber numbers as they have different fluid properties.

For each fluid used in this experiment, there was an entirely new fluid system used to prevent cross contamination. The fluid system consisted of the syringe, tubing, needle, and connectors. The needle was the only component that was not swapped out each time, but because of this, several drops were run through the needle before recording any data to allow the previous fluid to be completely flushed out. Each fluid was stored in separate glass vials until their use. For water, deionized water was used to prevent the presence of ions or contaminants from effecting the fluids behavior.

Number of videos saved for each droplet and height combination varied. The better that particular combination of fluid and release height were known the less videos needed to be saved for them. The combinations that were less well known or understood had more videos saved to just have a larger sample size. Some of those newer combinations also had variability to them, which necessitates extra samples to capture the extent of that variability.

After the data video was captured it was examined to determine if the data was good or not. This determination came down to two factors. The first factor was how well was the droplet impact centered in the frame of the video. If the droplet was too far off to the side, then some dynamics could be missed, and another video would need to be taken after the proper adjustments were made to realign the experiment. The second factor was if the droplet made contact in an unexpected manner, was that the result of a contamination such as a speck of dust being present on the surface of the oil layer. The speck of dust could be seen by the TIRM technique as a small, local dark spot that was present before the droplet came into view of the TIRM.

The camera used to record the droplet impacts was a Photron NOVA S9 at 32,000 fps. The camera framerate was selected as the fastest frame rate available for the resolution of 512x480 pixels, as this was the appropriate size to capture the entire droplet impact in the video. The corresponding maximum frame rate was 32000 frames per second. The shutter speed of the camera was selected based on the proper exposure of the image and intensity of the light source used. The light source was always set to the maximum output for all the experiments to be as consistent as possible. The intensity of the LED output did slightly affect the wavelength of the light emitted, which is a critical

variable for TIRM. Setting the output intensity to 100 percent every time ensured the light was also the exact same wavelength every time. The wavelength could be determined based on the output intensity from tabulated data from the manufacturer Thorlabs. With the light source always at maximum output, the shutter speed was adjusted to achieve the best expose for the image. If the image was over exposed then the TIRM did not align with reality anymore, and if the image was under exposed then the TIRM was less sensitive because it was only dealing with a small portion of the intensity distribution. Through trial and error and multiple sets of validation data the proper shutter time was determined to be 1.25 microseconds for this specific experimental apparatus. This shutter speed was still fast enough to prevent any motion blur in the frames of the video. The camera was also set to trigger at the end of the video. This was done out of consistency, as with such a high frame rate there was only a narrow window of actual video recording. Setting the triggering to the end allowed the largest possibility of capturing the entire droplet contact process with the human reaction time. The trigger was pulled as soon as the droplet hit the substrate. The video file was then cropped frame wise to only include the relevant frames as the droplet dynamics contained roughly an order of magnitude less frames than the entire length of the video. Then the video was saved as a tiff file for lens images and .avi file for droplet videos as both of these file types did not have any compression of information within the images or videos.

Fluid Properties

The fluids used in this experiment were selected primarily for their vapor pressures and accessibility. The three main fluids being water, ethanol, and acetone were chosen with water being the baseline, ethanol having roughly double the vapor pressure

of water, and acetone having roughly ten times the vapor pressure of water. All of these fluids are also easy to attain and work with.

Because of the large gap in vapor pressure between acetone and ethanol, two acetone-water mixtures were made. Mixture 1 was 1/3 water and 2/3 acetone by volume, and mixture 2 was 2/3-water-and-1/3-acetone by volume. The resulting molar fractions were 12.2% acetone for mixture 1 and 35.8% acetone for mixture 2. In order to create the mixtures, a separate syringe was used to extract a precise volume of each fluid. The syringe was weighed prior to being filled, once full of the liquid, and after releasing the liquid into the mixing container. The scale used measured the weights of each measurement to 0.1 mg of precision, so this method was used over the 0.1 mL uncertainty of the syringe. With the densities of acetone and water being $784 \frac{\text{kg}}{\text{m}^3}$ and $997 \frac{\text{kg}}{\text{m}^3}$ respectively, the weight measurements were 784 and 997 times more precise, respectively. Before each experimental session with the mixtures, the container with them was shaken vigorously to ensure a homogenous mixture.

The key fluid properties for this experiment are the density, dynamic viscosity, surface tension, and vapor pressure. These values for the pure water, ethanol, and acetone are readily available, but these values for the acetone-water mixtures are less available. For the vapor pressure values of these mixtures, Raoult's law was utilized. It calculated the vapor pressure of the mixture by summing the vapor pressures of each fluid weighed by their mole ratio in the overall mixture. Summary information for the fluids used is provided in table 3.1 below.

Table 3.1 Droplet Fluid Properties

Fluid	Density ($\frac{kg}{m^3}$)	Dynamic Viscosity ($mPas$)	Surface Tension ($\frac{N}{m}$)	Vapor Pressure (kPa)
Water	997	1.002	0.0729	2.3
Ethanol	789	1.184	0.022	5.3
Acetone	784	0.316	0.025	25
Mixture 1	890	0.550	0.0287	10.4
Mixture 2	956	0.366	0.0366	5.1

Drop Size Validation

This validation experiment was setup differently from the droplet impact experiment as TIRM is not used for this validation experiment. The goal of this validation experiment was just to image the droplets as they fell through the air, in order to measure their diameters precisely to feed back into the Weber Number values for the droplet impact data. The light path to the camera was positioned just below where the droplets were released from, to ensure the entire droplet would be captured in the image before it fell below the view of the camera, as the further it falls the faster it falls. A phantom camera used for this validation experiment. An LED and collimating lens were also used to illuminate these videos, in a very similar manner as the main experimental setup. The wavelength of the light was not relevant for this validation experiment, as all that was required was illumination of the droplets, so the shutter speed and LED intensity were not locked into specific values. The same camera settings and rough LED intensity were used throughout all the validation videos for consistency. The phantom was set to 2200 frames per second, 60 microsecond shutter speed, and resolution of 1280x800 pixels. The resolution was maxed out for this frame rate, in order to capture the largest image area. The frame rate was selected as the slowest frame rate that still had the

droplet at least partially in view for several frames, as the slower the frame rate the larger the resolution can be. Also, it is important to note that with the 5x objective lens assembly attached to the camera, the water droplets nearly spanned the entire height of the image domain with the 1280x800 pixel setting. The camera was still set to trigger the video at the end, to give the human operator the maximum reaction time to record the droplet as it passed the camera's view. An example image of one the droplets captured in this method is depicted below in figure 3.1.

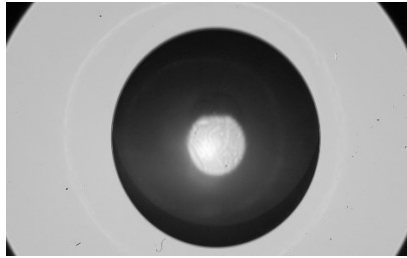


Figure 3.1 Raw drop size images: mixture 1

A code was developed to take in the droplet images and determine the actual diameters of the droplets. First a threshold is applied to the image to create a binary image for “regionprops” to work with. Then “imfill” is used to fill in the center of the droplets as they all have a bright spot, and “regionprops” thinks the bright spot is a separate body. Then “regionprops” measures the major and minor diameters as well as the centroid of the droplet. The major and minor diameters are then averaged to find the radius of the droplet if it was a circle. Note that the droplets are slightly elliptical from the oscillations they experience from their departure from the needle. Then a circle is plotted on top of the droplet image, with the centroid and average diameter as described above, to ensure the right object was identified and the circle measurements are accurate. The diameters of each grouping of droplets by fluid is averaged and output for the use in

the Weber Number calculations. Some examples of the identification of the droplet are visualized below in figure 3.2, with the summary results of this analysis in table 3.2 below.

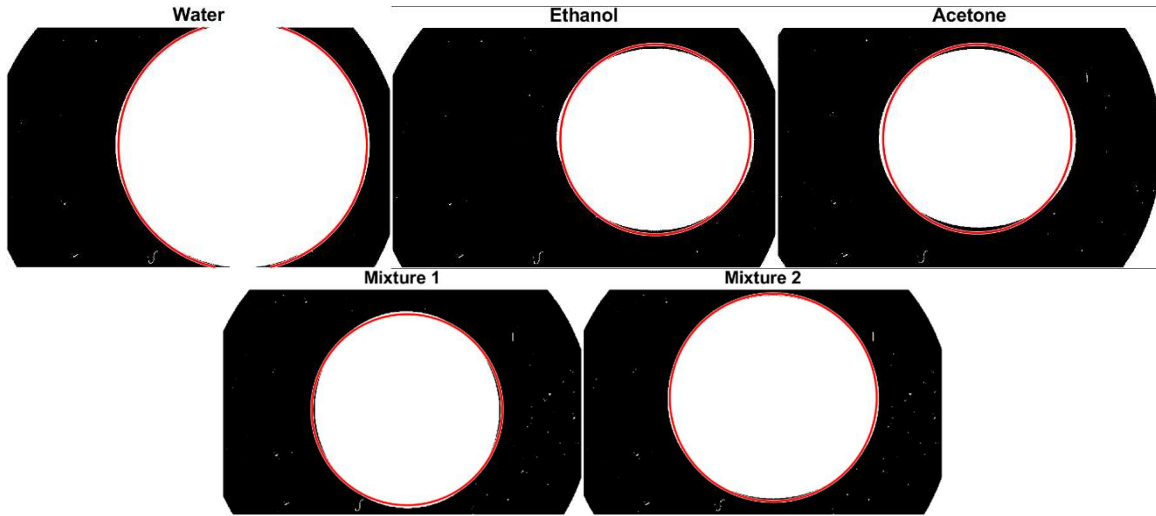


Figure 3.2 Droplet diameter measurements

Table 3.2 Droplet Diameter Summary

Fluid	Average Diameter (mm)	Uncertainty (mm)
Water	2.16	0.0078
Ethanol	1.67	0.0011
Acetone	1.68	0.0191
Mixture 1	1.79	0.0148
Mixture 2	1.96	0.0028

CHAPTER FOUR

Results and Analysis

Pre-Contact Analysis

Taking the droplet videos and analyzing the air film prior to contact is critical to understanding the mechanism for contact or air film failure. The following figures correspond to a representative video for that droplet's behavior for its Weber number. The videos were selected to have as similar Weber numbers as possible, to allow the difference to be solely from the difference in vapor pressures between the fluids. Figures 4.1 through 4.5 are in order of increasing vapor pressure or volatility, to demonstrate the effect of vapor pressure on the air film temporal progression. Note that the water and ethanol impacts at this We number bounced, and so the profiles for pre-contact analysis stop tracking the air film once the droplet has stopped spreading and starts receding. Both of the mixture impacts, and the acetone impact all made contact at this We number, so the videos were stopped once contact occurred to prevent all the data points along the bottom edge cluttering up the plots. The profile location for each droplet starts at its center and traces out a straight line directly upward to the top of the image. The profiles are not radial averages. They are just a single profile slice of the air layer for each droplet. Figures 4.6 through 4.10 correspond to figures 4.1 through 4.5 respectively, with the difference being the y axis is now the normalized droplet height as determined by the TIRM equations 2.1 through 2.21.

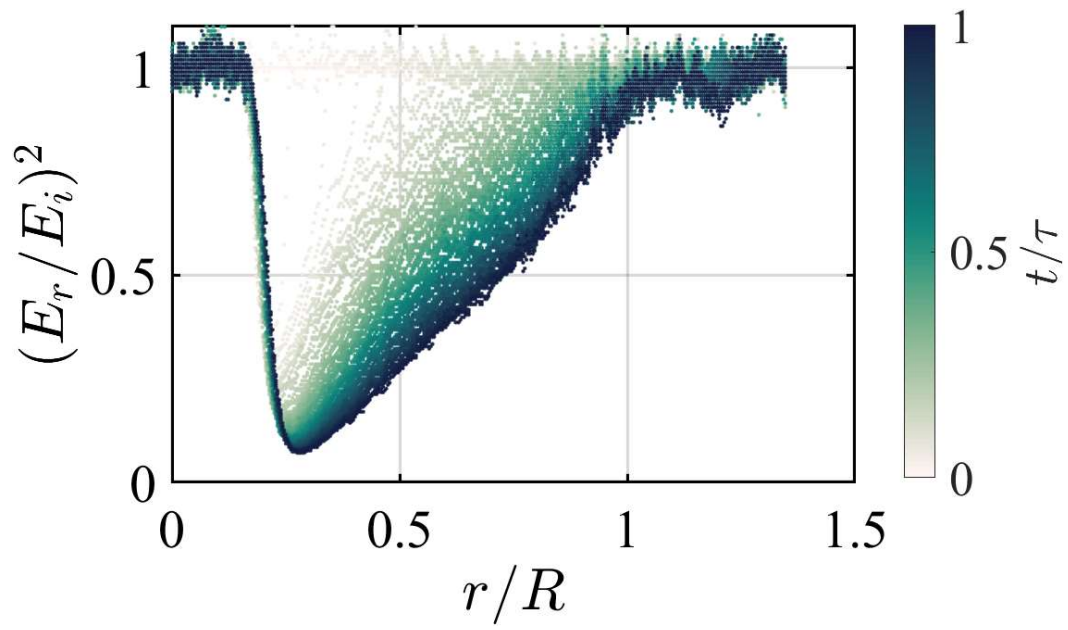


Figure 4.1 Pre-contact water reflectance vs normalized radius

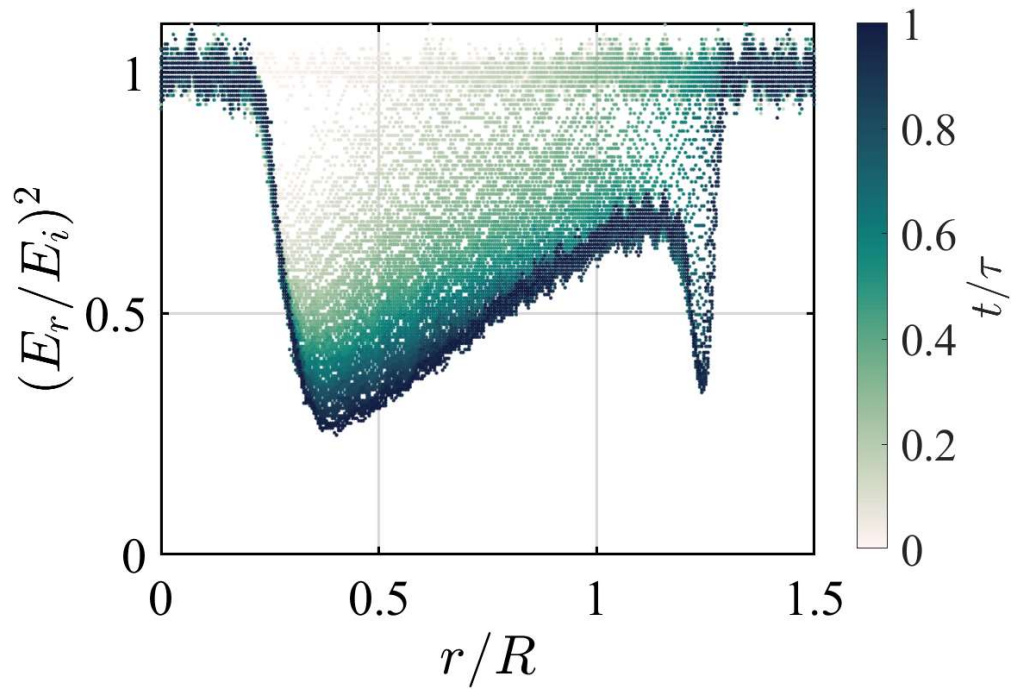


Figure 4.2 Pre-contact ethanol reflectance vs normalized radius

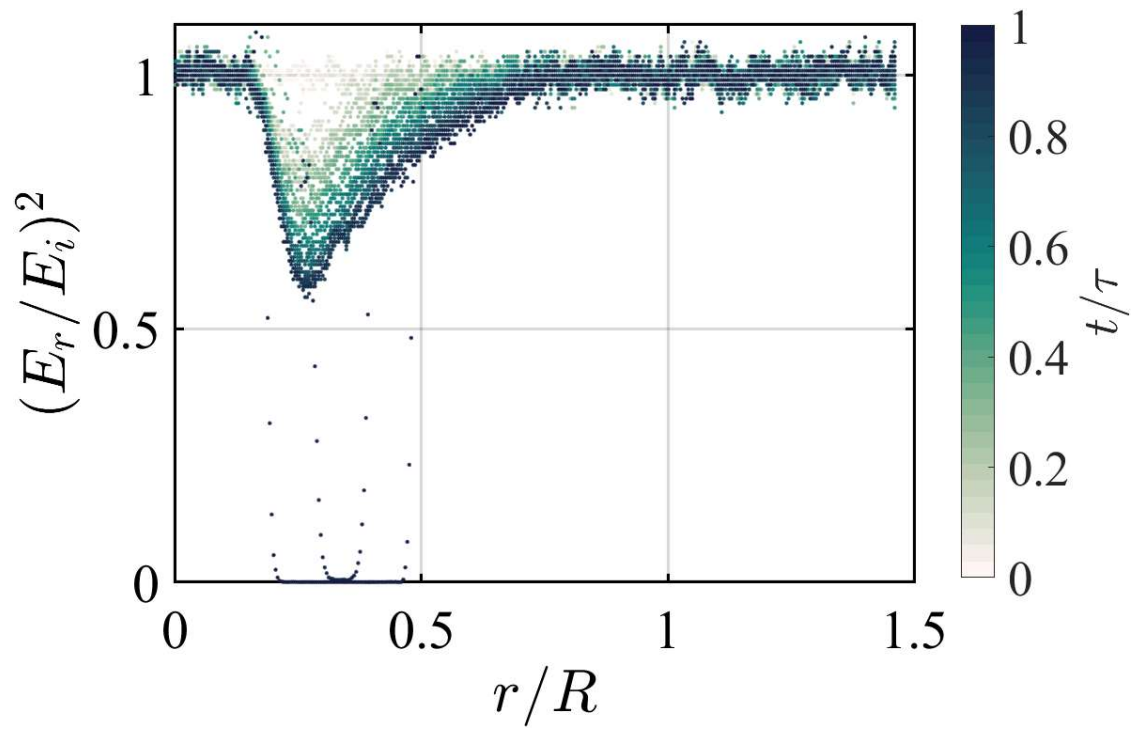


Figure 4.3 Pre-contact mixture 2 reflectance vs normalized radius

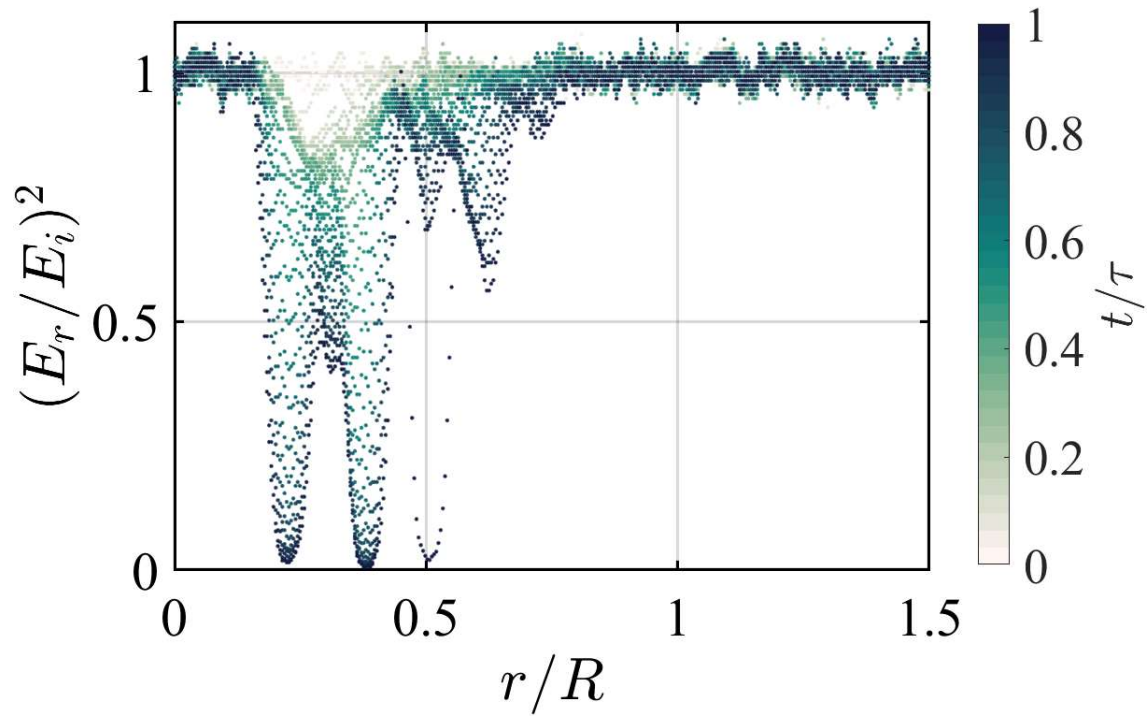


Figure 4.4 Pre-contact mixture 1 reflectance vs normalized radius

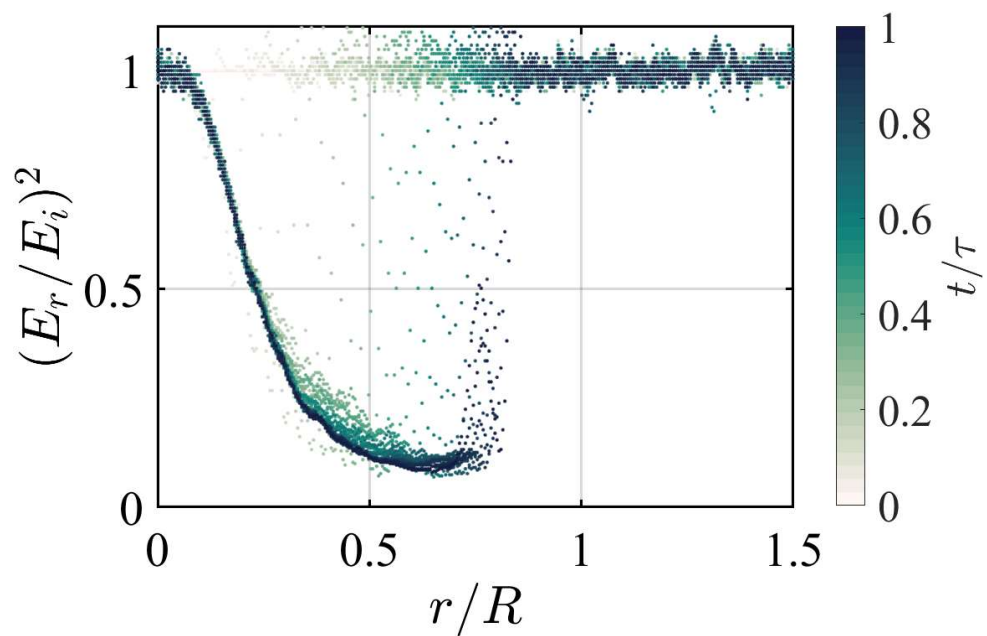


Figure 4.5 Pre-contact acetone reflectance vs normalized radius

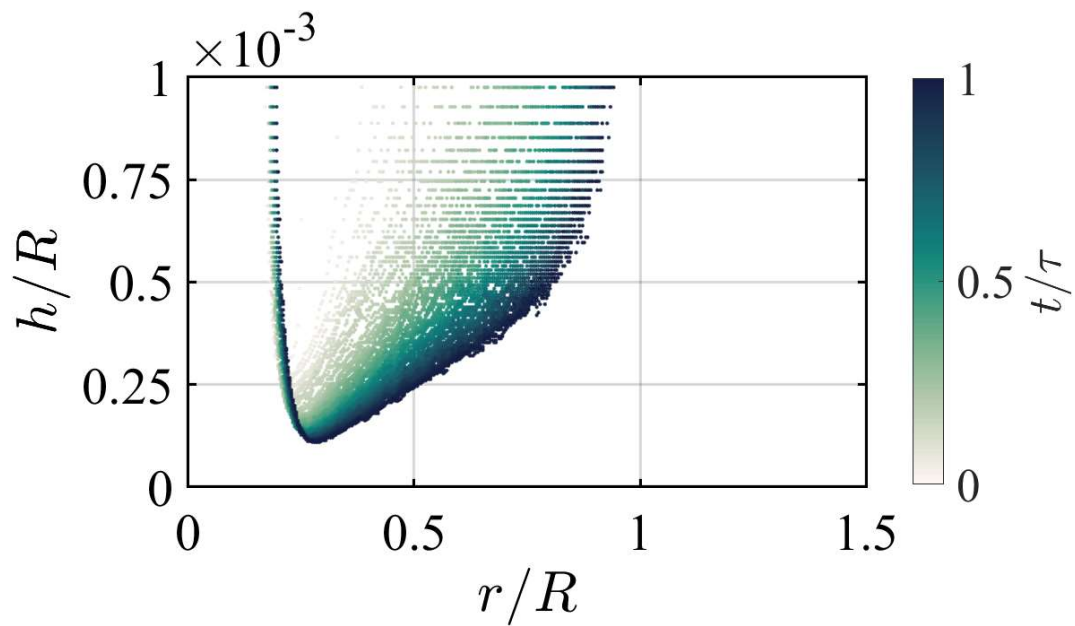


Figure 4.6 Pre-contact water normalized air film height vs normalized radius

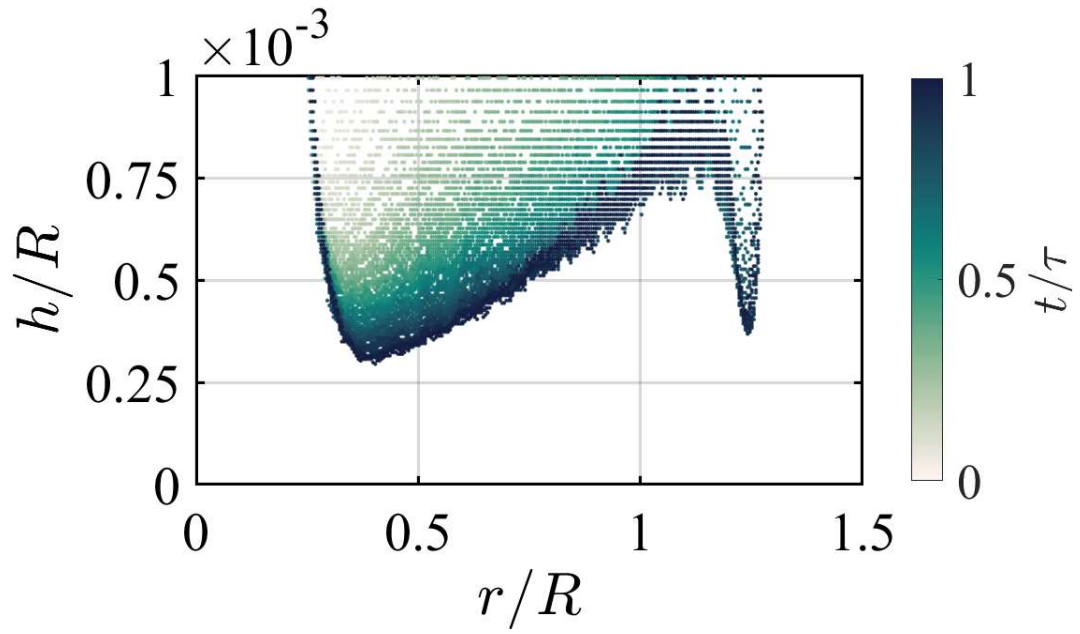


Figure 4.7 Pre-contact ethanol normalized air film height vs normalized radius

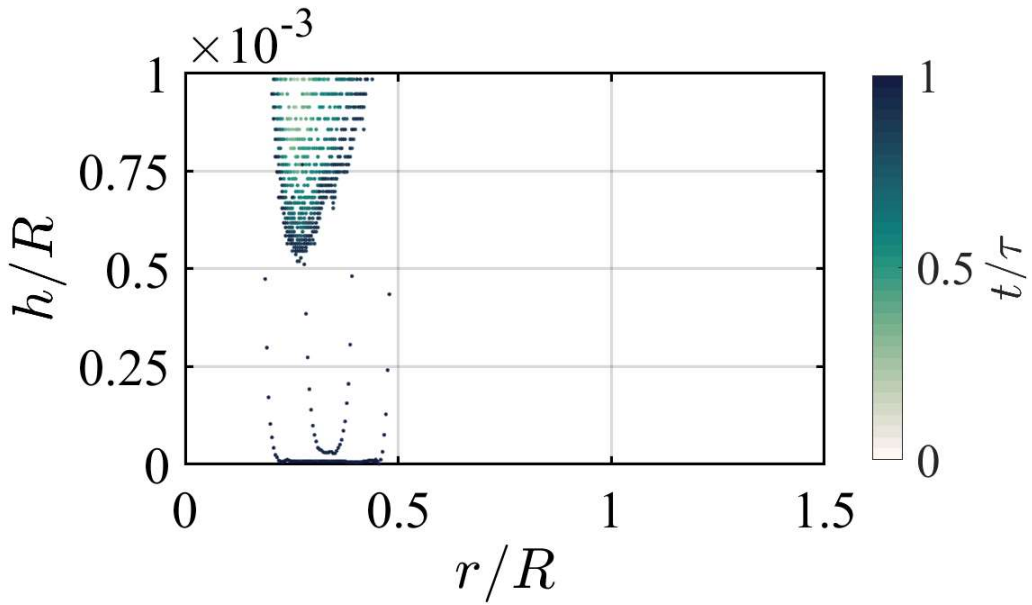


Figure 4.8 Pre-contact mixture 2 normalized air film height vs normalized radius

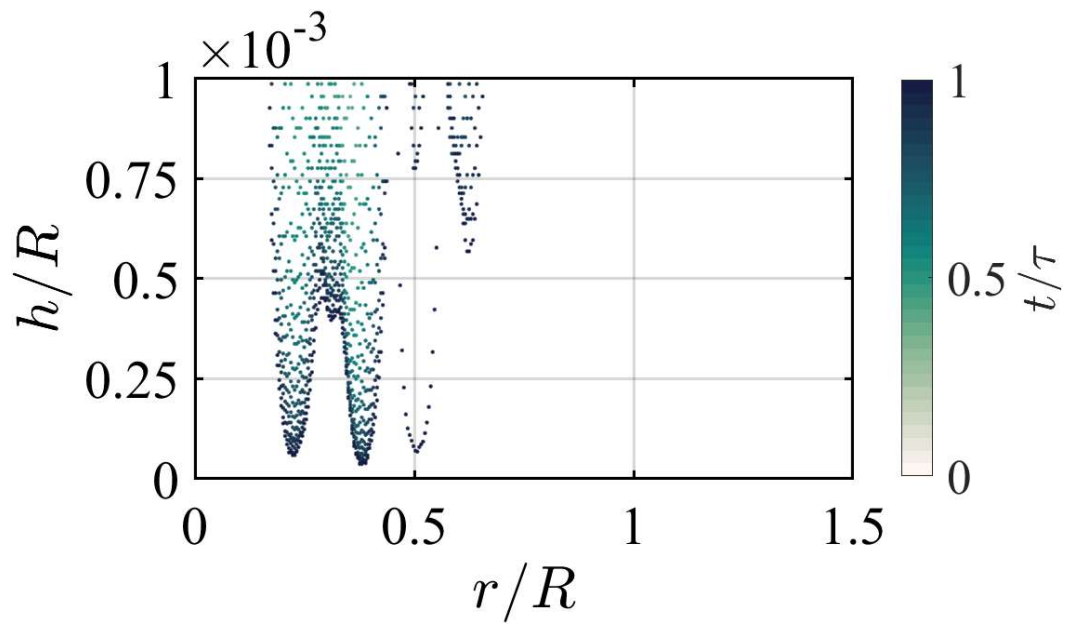


Figure 4.9 Pre-contact mixture 1 normalized air film height vs normalized radius

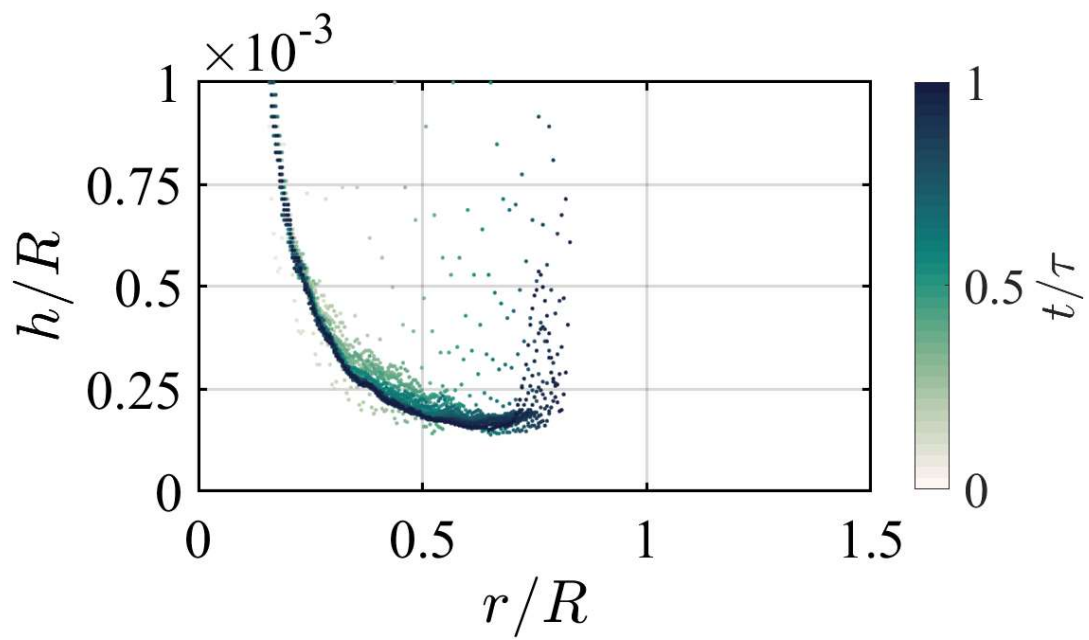


Figure 4.10 Pre-contact acetone normalized air film height vs normalized radius

Contact Visualization

With the video recordings generated from the TIRM experimental apparatus described previously, the shape of the droplet just above the substrate is visualized. One of the first common aspect of these videos that an observer notices, is the sudden black dots that form and usually expand radially and rapidly compared to the rate of change of the droplet shape throughout the rest of the video. These black dots are locations where the droplet is contacting the substrate.

Contact locations, as visualized with TIRM, have three main characteristics. The first is a cluster of nearly black pixels. In most experiments, the nearly black cluster will also have a narrow white border around it. Lastly, the contact patch will rapidly expand radially as the droplet wets the substrate. The contact patch's radial expansion will occur several times faster than the spreading of the air film, and quickly encompass the entirety of the air film. Between these characteristics, it is possible to distinguish contact points from other dark regions in the air film profile.

In figure 4.11 below there is one image sequence for each fluid. The fluids are depicted in the following order, from the top row down to the bottom row: Water (We 14.5), Ethanol (We 29.2), Acetone (We 25.9), Mixture 1 (We 27.2), and Mixture 2 (We 25.1). Each fluid image sequence contains images separated by a single frame. The first frame where the droplet contacts the substrate is identified with a red border. In order to ascertain which frame the acetone droplet made contact, the image was zoomed in and examined closely. The acetone and ethanol droplets do not always have a white border around the contact points.

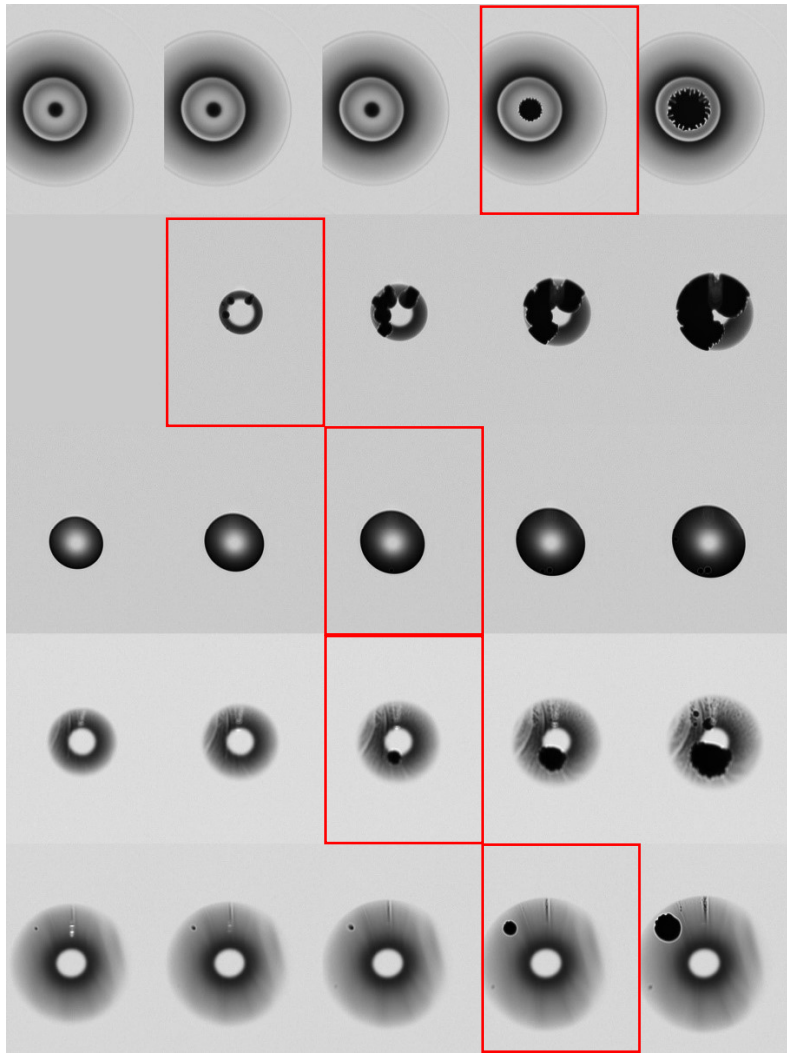


Figure 4.11 Finding contact frame

The droplets do not always contact the substrate. The Weber number is a key metric used to anticipate if a droplet will make contact or just bounce. Sometimes a droplet can make a small point of contact and still bounce away. Near the boundary of bouncing or contacting ($We = 5-10$), some droplets will contact, and some will bounce despite being on the wrong side of the threshold. See tables 4.1 and 4.2 below for the Weber number breakdown and a summary of how many droplets made contact and which condition set they fell under respectively for the data collected in this experiment.

Table 4.1 Release Height to Weber Number

Release Height (cm)	Water	Ethanol	Acetone	Mixture 1	Mixture 2
0.5	2.9	5.8	5.2	5.4	5.0
1.0	5.8	11.7	10.3	10.9	10.0
1.5	8.7	17.5	15.5	16.3	15.1
2.0	11.6	23.4	20.7	21.8	20.1
2.5	14.5	29.2	25.9	27.2	25.1
3.0	17.4	35.1	31.0	32.7	30.1
3.5	20.3	40.9	36.2	38.1	35.1
4.0	23.2	46.8	41.4	43.5	40.2

Table 4.2 Summary of Experiments with Contact

Release Height (cm)	Water	Ethanol	Acetone	Mixture 1	Mixture 2
0.5	1/4	0/4	2/5	7/9	7/10
1.0	0/3	3/6	4/4	9/9	10/10
1.5	2/3	4/4	8/8	10/10	10/10
2.0	1/3	4/4	6/6	10/10	10/10
2.5	3/3	5/5	6/6	9/9	10/10
3.0	3/3	4/4	6/6	10/10	10/10
3.5	3/3	4/4	7/7	10/10	10/10
4.0	3/3	4/4	6/6	10/10	10/10

The Weber numbers were calculated with the velocity of the droplet at impact being predicted from the potential energy to kinetic energy conversion ignoring air resistance. All that was needed for the velocity was the release height of the fluid. The droplet diameters from the methodology section were used for the length variable. The surface tensions and densities correspond to their values listed in table 3.1.

Figures 4.12 through 4.16 are images of the droplets a few frames after initial contact with the substrate. This is to illustrate the typical contact appearance under each respective condition as the contact patches grow enough to be readily noticeable.

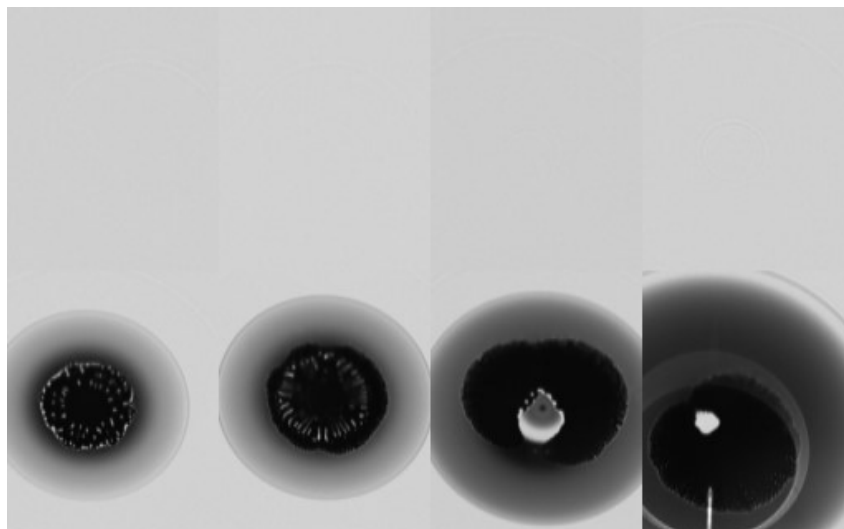


Figure 4.12 Typical water contact

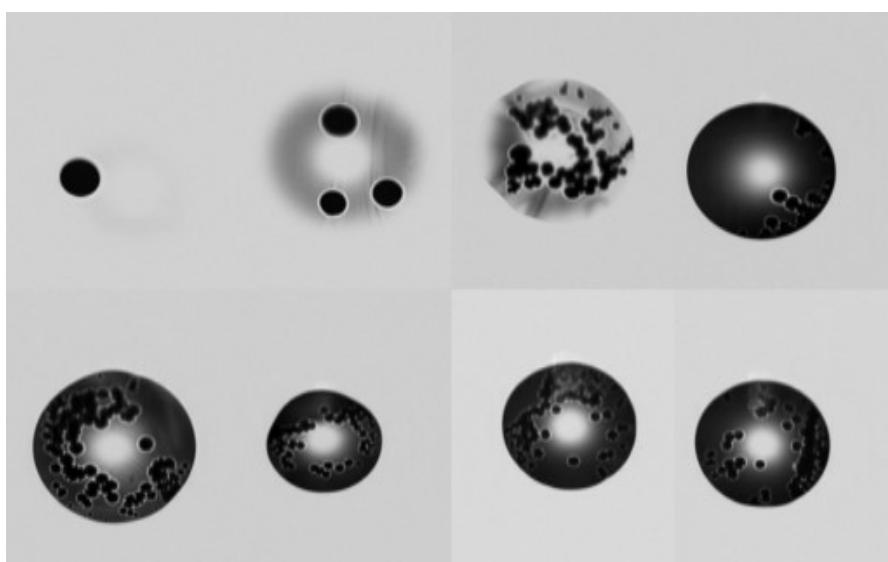


Figure 4.13 Typical acetone contact

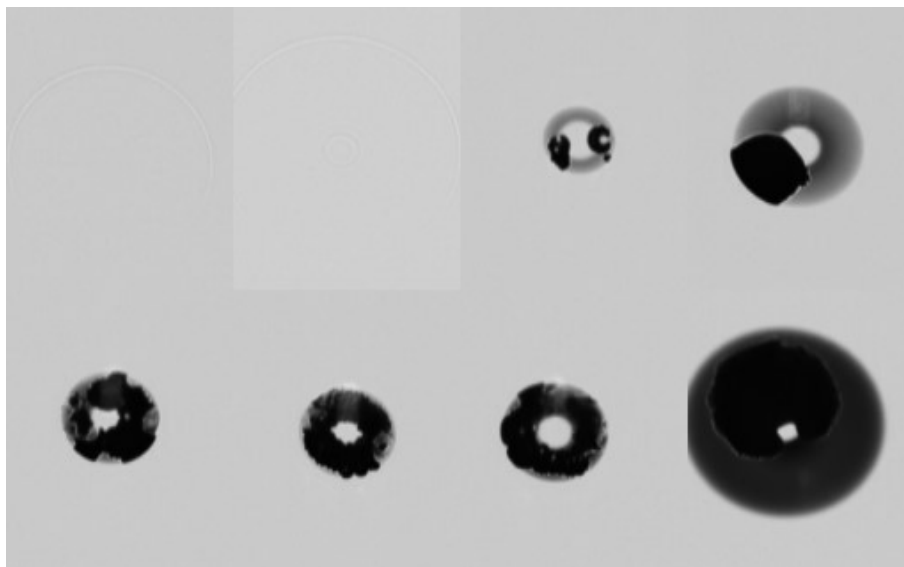


Figure 4.14 Typical ethanol contact

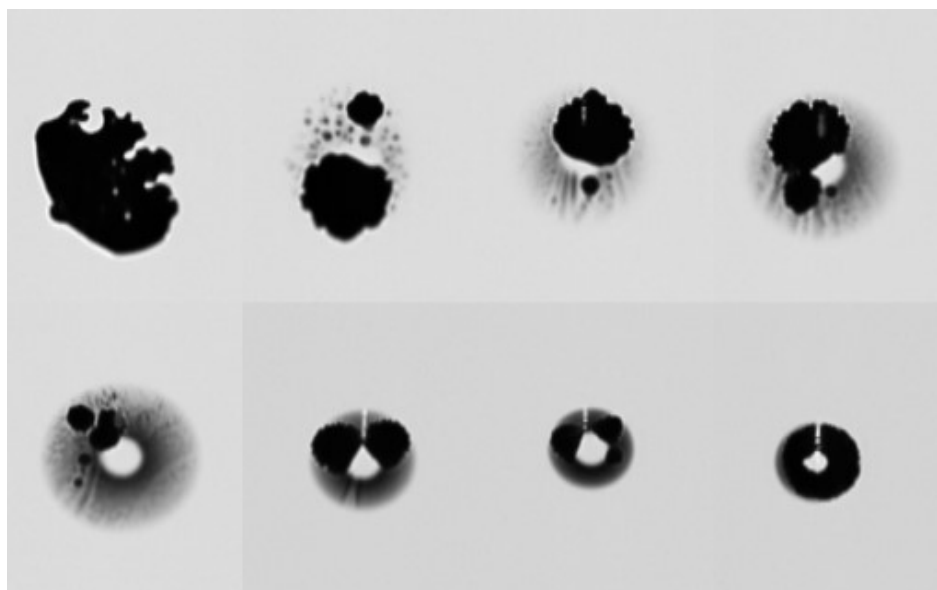


Figure 4.15 Typical mixture 1 contact

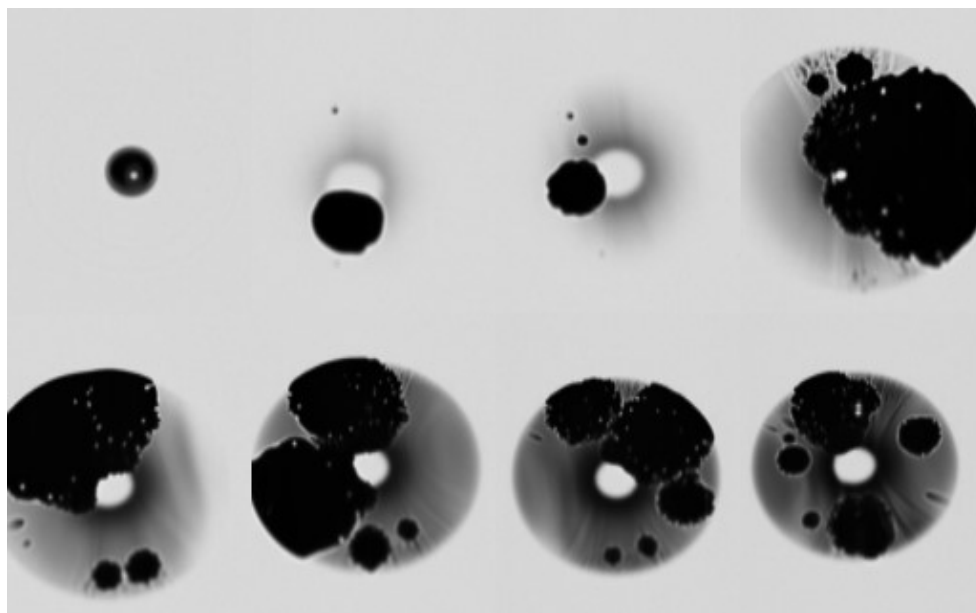


Figure 4.16 Typical mixture 2 contact

All of the figures above depicting the typical contact patterns of the various droplets are sorted in ascending order of their corresponding Weber numbers. The water droplets are very simple and often make one point of contact very close to the center of the droplet. Acetone droplets make contact at lower Weber numbers and usually with several individual points of contact. Ethanol makes contact at the same Weber number range as water. Much like acetone, ethanol typically has multiple distinct contact points, but unlike acetone, the contact points are not circular in nature and are quite irregularly shaped. Mixture 1 (1/3 water - 2/3 acetone by volume) droplets are similar to pure acetone, as these drops contacted at lower Weber numbers than pure water. The drops also have noticeably more variation in their height, looking at the second image in this sequence shows many dark spots relative to the overall droplet darkness. The contact can also be more irregular, like ethanol droplets. Mixture 2 (2/3 water - 1/3 acetone by volume) is much more stable than mixture 1, as the darkness of the overall droplet is

more even. There are almost streaks of relative brightness in the drops though. The drops still contact with multiple distinct points, but the points themselves are fairly circular.

With the data that has been shown, as the vapor pressure increases, the contact patterns become more chaotic. The air film failures for water droplets occur either precisely in the center or on the edge of the dimple, which agrees with the conclusions from Pack et al's paper [2]. However, the air film failures for the other fluids occur in the flattened, lower height portion of the air film, away from the dimple. As the vapor pressure increases, either the air film becomes more unstable with wide fluctuations between bright and dark spots as is seen in the mixtures, or there is a dramatic increase in the number of contact points (as will be discussed more later) with the acetone droplets.

Data Quality

There are two cases for the data to be thrown out. Either the droplet impacted onto a contaminant that disrupted the air layer stability or there was too much noise in the image to begin with.

To determine if a contaminant is what caused the air layer failure, the videos must be viewed prior to background subtraction, as the background subtraction removes any contaminants from view. Figure 4.17 is an example of a video with potentially significant contaminants. What should be looked for is the presence of a dark spot in the background image that correspond to the exact location of the initial point of contact between the droplet and the substrate.

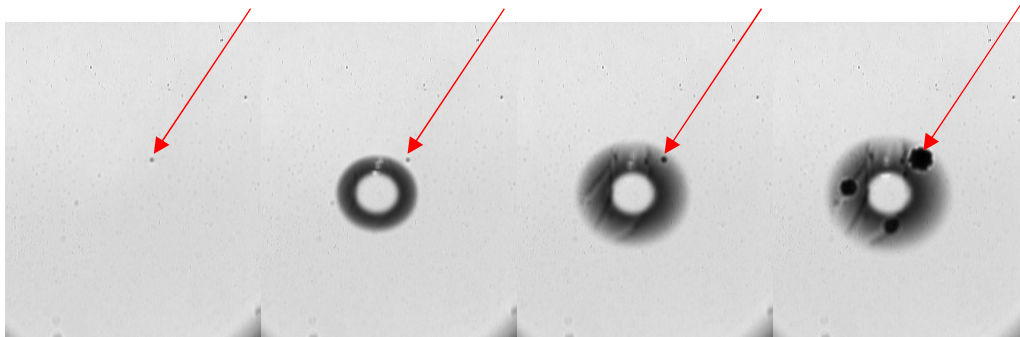


Figure 4.17 Contact routes on contaminated surfaces

This is an example of a contamination leading to contact prematurely. Just beyond the top right corner of where the droplet initially appears, there is a dark speck. This speck is at the end of the red arrow superimposed over the images. That speck perfectly overlaps with one of the initial contact points. That resulted in this specific video being removed from the data analysis. The speck was present in the image sequence prior to the droplet coming into view, and the first contact point perfectly overlaps the position of the speck. Because of this, it is impossible to determine if the air film naturally failed coincidentally in the location of the speck or if the speck represents a piece of dust that fell onto the oil layer prior to the experiment, and that dust caused the rupture in the air film.

The goal of the background subtraction is to provide a cleaner view of the droplet and its structural changes over time, as small bubbles typically form in the immersion oil layer between the glass slide and the prism, and these bubbles disrupt the light path and produce dark spots in the image. It is noted that when a video is background subtracted the pixel intensities now range from 0 to the pixel intensity in the corresponding background image used. So, for the pixels covering the regions of these darker bubbles, less information can be contained as the intensity range is significantly decreased. When

the droplet does come into view, the pixels in the image that were already dark remain dark, and therefore after background subtraction are bright and remain bright despite the droplet being present. If there are too many dark spots, then there could be a significant loss of information in the resulting analysis. Figure 4.18 below gives some examples of common obscurities in some of the videos.

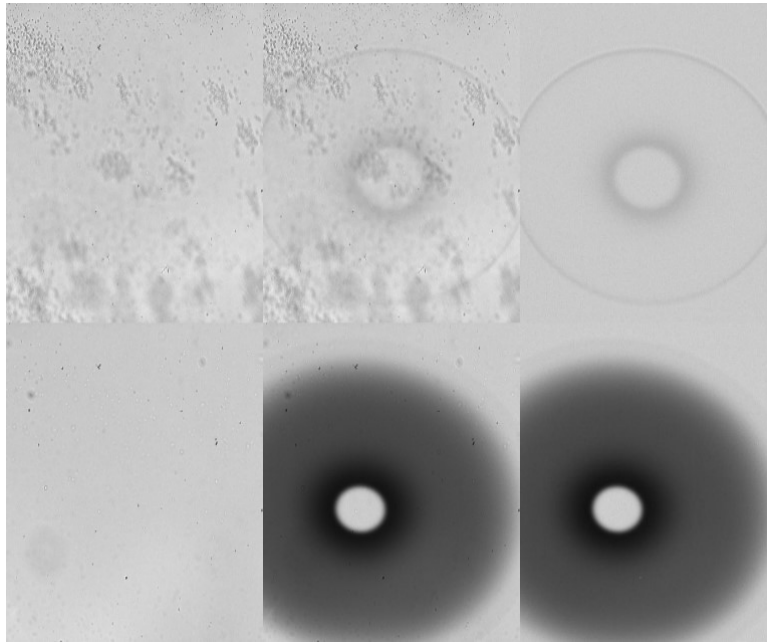


Figure 4.18 Potential visual obscurities

Each row contains the same information, just for different release heights of water videos. The first image is the background image of the video, the second image is a frame that captures the full droplet, and the third image is the same frame of information as the second image after background subtraction. The top row clearly has an excessive number of bubbles in the oil layer, but as it was dropped from a lower release height, the visualization from the TIRM contains only a couple rings of information that are not significantly disturbed. The bottom row has less bubble influence but has been released

from a higher release height. This results in there being more of a gradient of information to be analyzed. In this gradient the background subtracted image does not have any evident spurious data from the background noise or bubbles. Both of these videos remained in the data analysis as the information they contained was determined to be unimpeded by the presence of the bubbles and other optical contaminants. Figure 4.19 below has one example from the videos of each fluid group used in the experiment in the usual order of water, ethanol, acetone, mixture 1, and mixture 2.

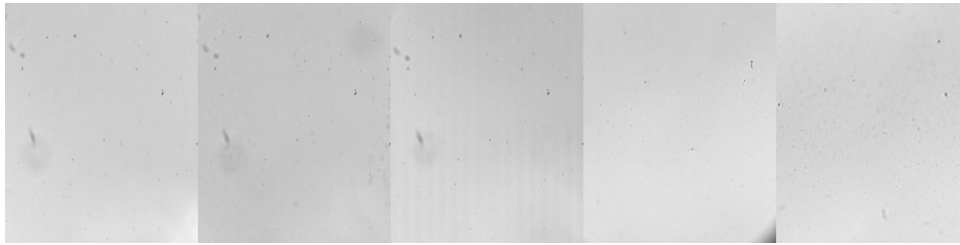


Figure 4.19 Typical video backgrounds

Initial Contact Time

The initial contact time simply refers to the amount of time between the droplet entering the view of the TIRM and its first recorded frame of contact with the substrate. In order to measure this value, the first frame of the video with the droplet affecting any pixels in the view is noted and the frame of first contact is noted. Then the number of frames can be subtracted from each other and when divided by the frame rate of the video recording the initial contact time is determined. Figure 4.20 below shows how both the first frame and first contact frame are identified relative to their surrounding frames. The first row shows the first frame the droplet comes into view as marked with the red outline, and the second rows shows the first contact frame as marked with the red outline.

The purpose of measuring the initial contact time is to assess how quickly the air film fails, to determine if the vapor pressure causes this failure to occur faster or slower.

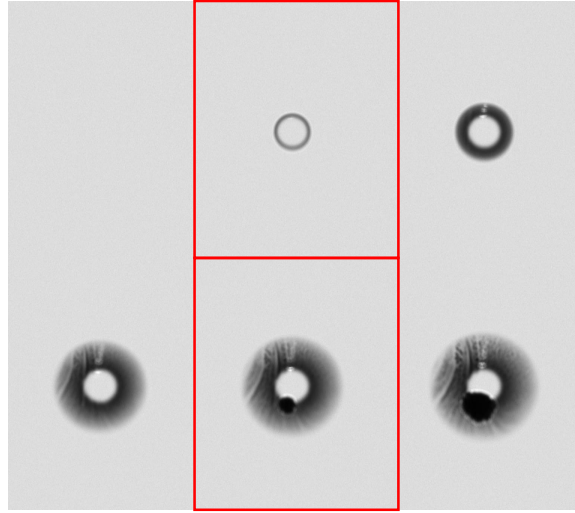


Figure 4.20 Initial contact time definition

Figures 4.21 through 4.25 below are comprised of the images of the initial contact frame for one of the data videos under each condition. The conditions being different release heights for different fluids. If there was no contact in the video, in other words the droplet bounced, then the last frame of the video is shown in its place.

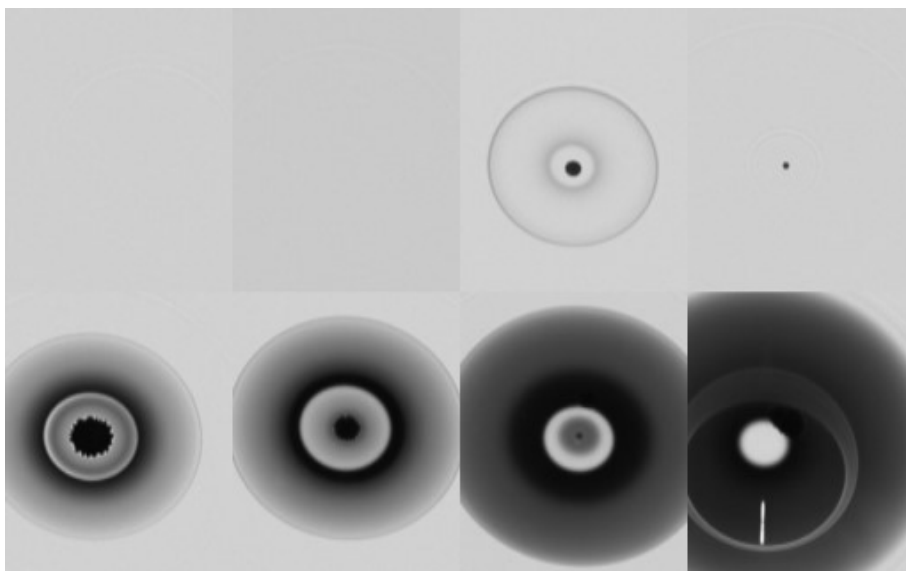


Figure 4.21 Initial water contact

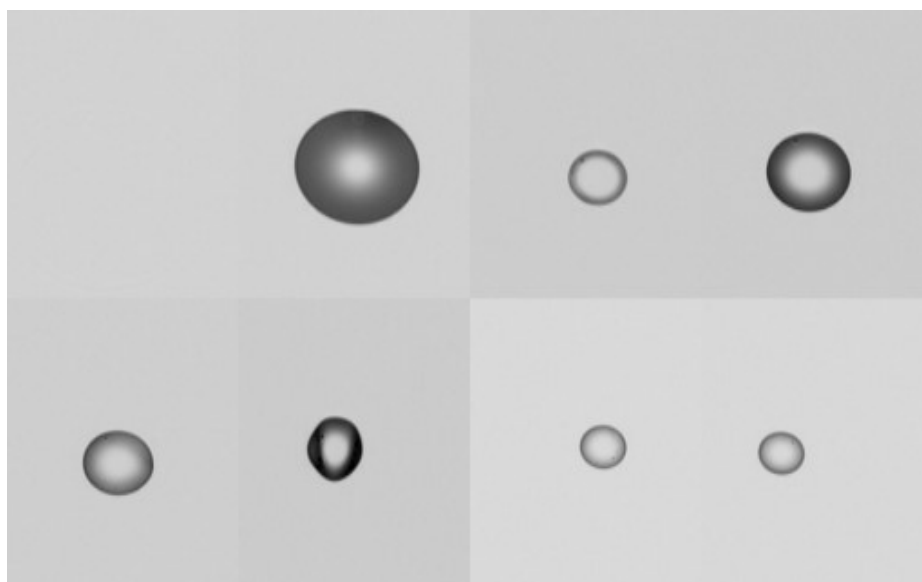


Figure 4.22 Initial acetone contact

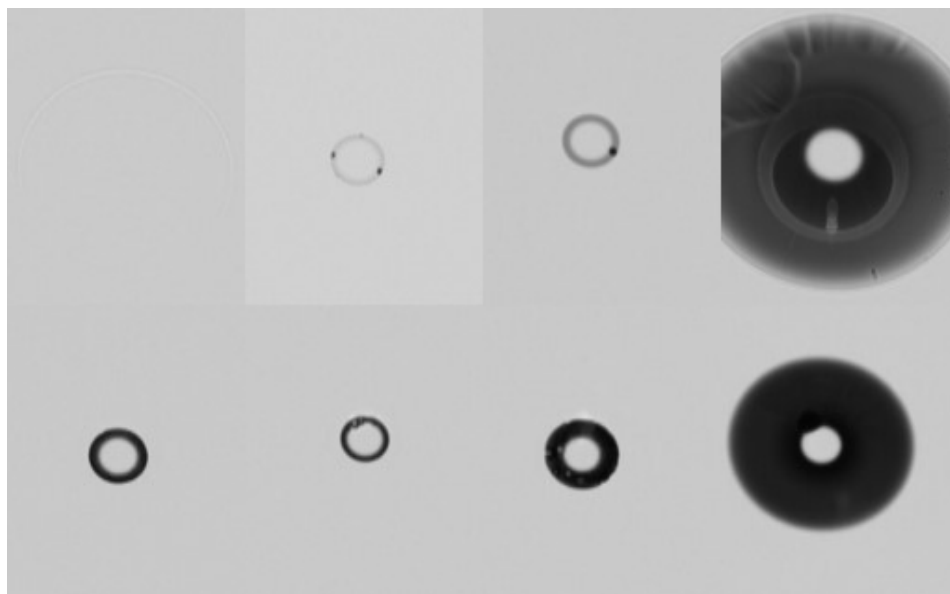


Figure 4.23 Initial ethanol contact

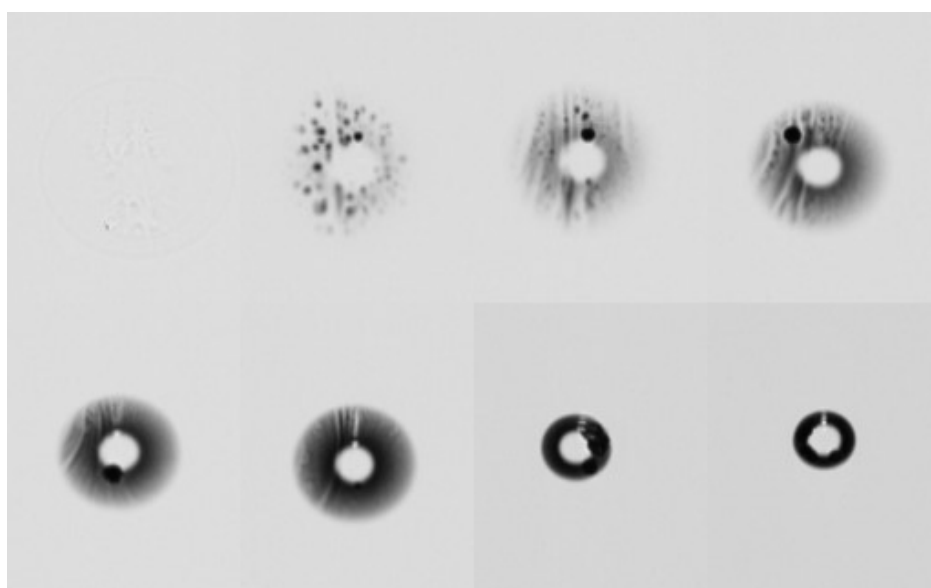


Figure 4.24 Initial mixture 1 contact

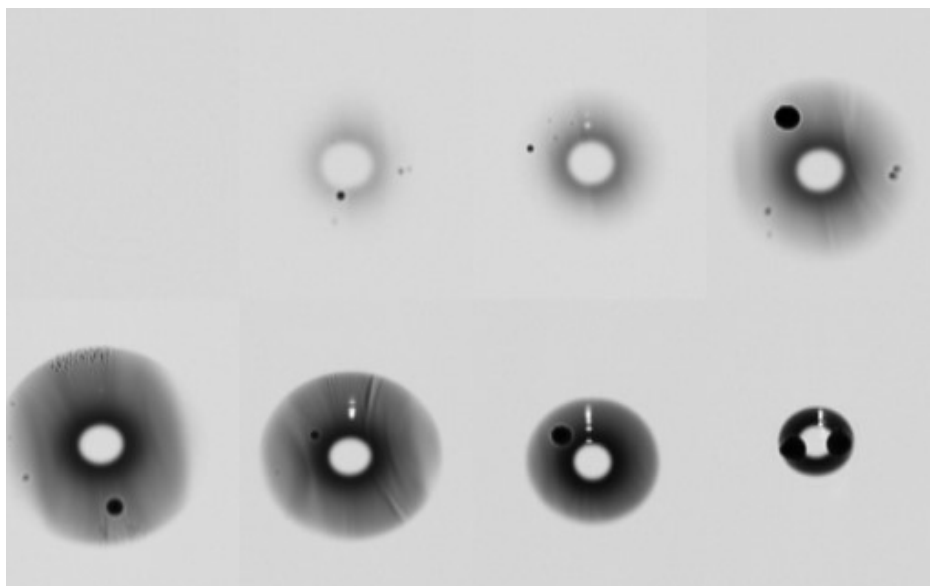


Figure 4.25 Initial mixture 2 contact

All of the figures above depicting the typical first frame of contact of the different fluid groups are sorted in ascending order of their corresponding Weber numbers. For water droplets, the initial contact is always on or near the center of the droplet. The initial contact for acetone is usually near the circumference or outer edge of the droplet, in opposition to water. Ethanol droplets have unpredictable initial contact as it occurs anywhere within the low height, flat portions of the air films and does not have a clear trend of occurring in an earlier phase of the droplet morphological process with an increase in Weber number as the fourth and eighth images indicate. Mixture 1 initial contact is unpredictable as to the typical location of initial contact relative to the center or edge of the droplet. The mixture 2 droplets' initial contacts occur within the low height, flat portions of the air films as with mixture 1.

Something to note is that water typically makes contact as the droplet is receding or at least done spreading, but acetone and ethanol droplets make contact as the droplets are initially spreading. Spreading or expanding here means specifically expanding how

much of the droplet is in view of the TIRM, as the bottom of the droplet deforms and flattens out due to the pressures in the air film.

All of the initial contact times are now depicted in figures 4.26 through 4.29 below. Comparing the times to both Weber number and the fluid's vapor pressure, is important as the Weber number is already known to affect contact of the droplet and substrate, and vapor pressure is the key parameter varied for this experiment.

Note that all scatter plots that have the vapor pressure as the horizontal axis also have constant We number curves displayed over the data. The We number values were interpolated, as the data points themselves do not always align with specific We numbers. These constant We number curves do not depict any more data points, they merely show how the We number progresses.

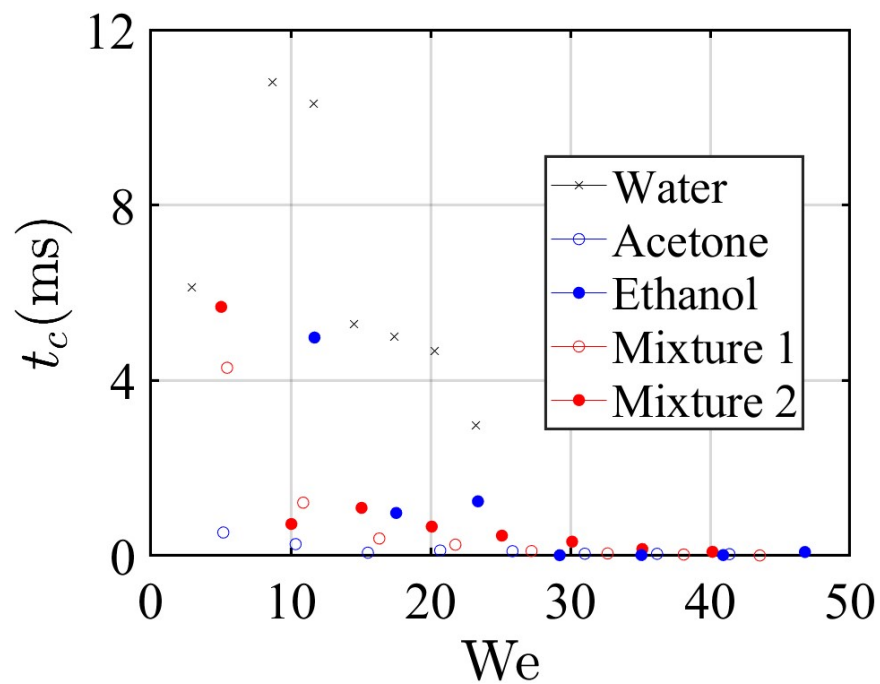


Figure 4.26 Weber number vs initial contact time

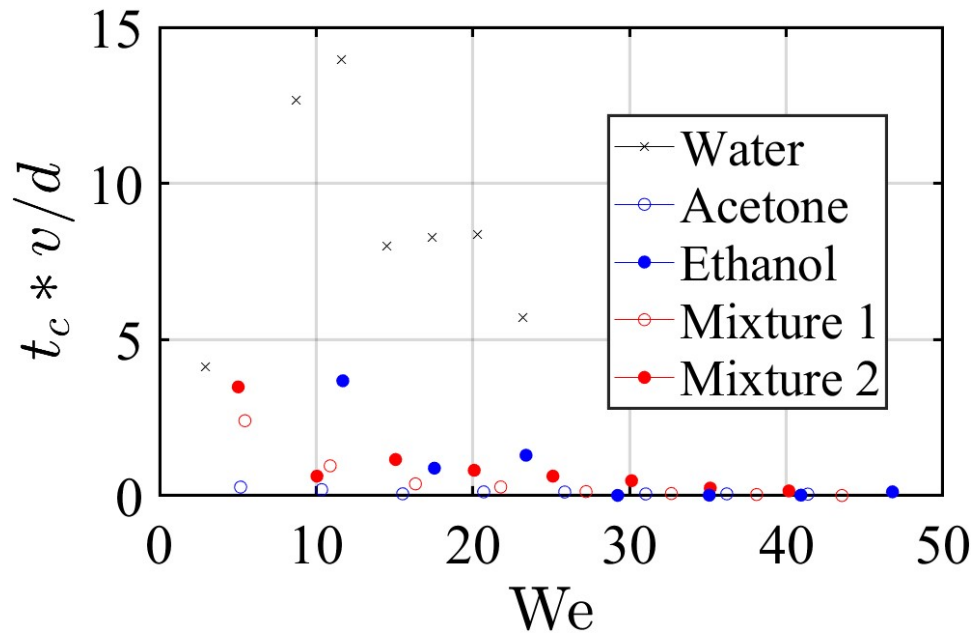


Figure 4.27 Weber number vs nondimensional initial contact time

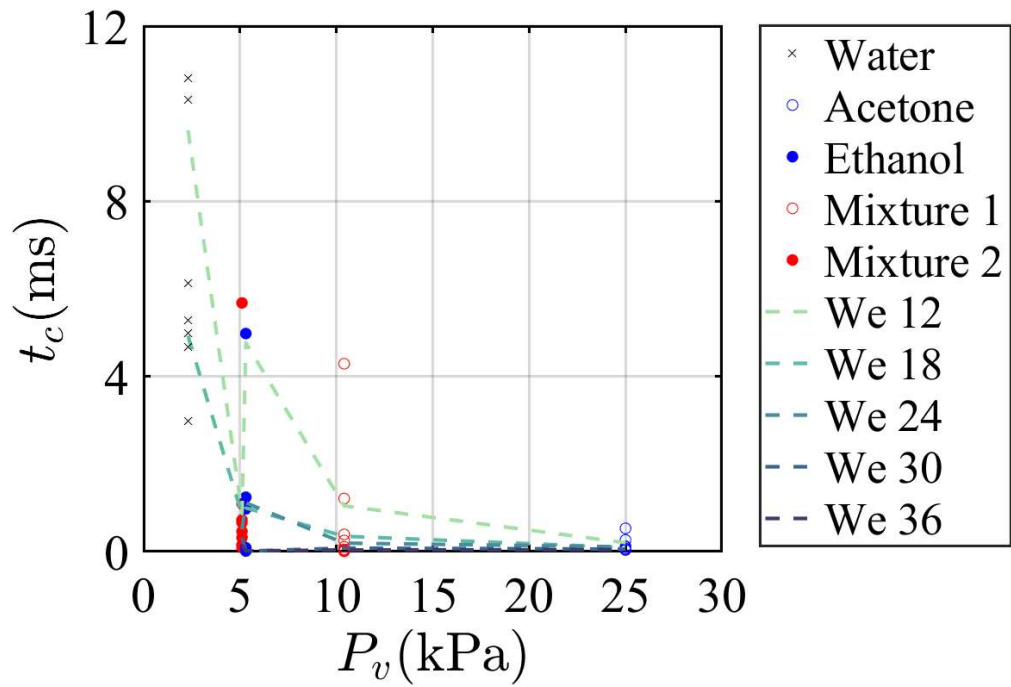


Figure 4.28 Vapor pressure vs initial contact time

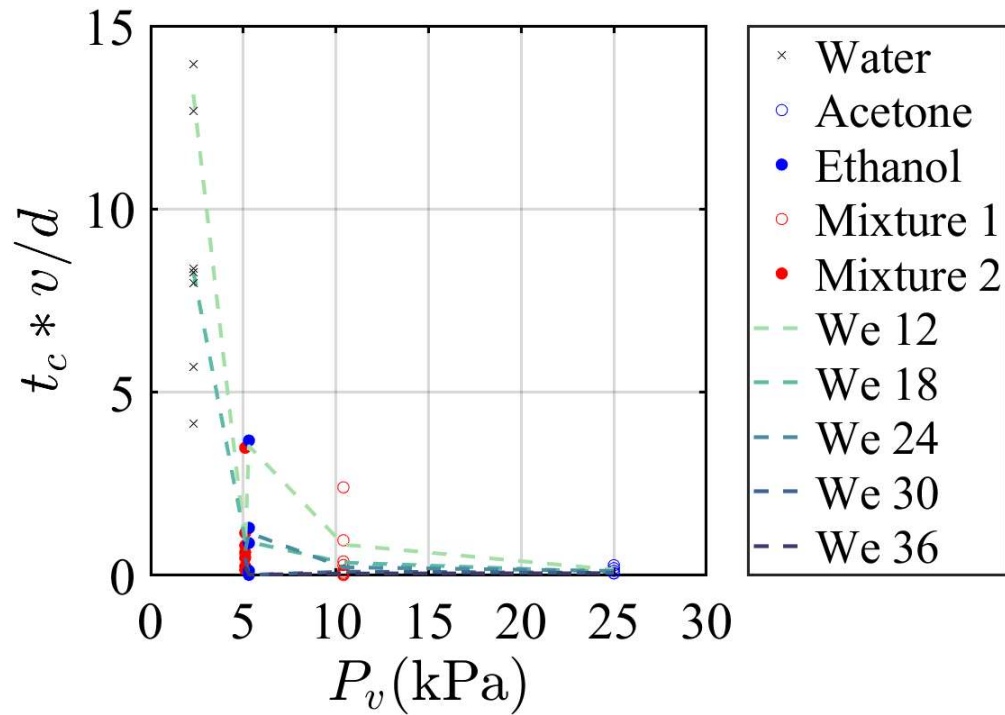


Figure 4.29 Vapor pressure vs nondimensional initial contact time

The initial contact time figures plot all the data's initial contact times versus Weber number and vapor pressure, respectively. If the droplet did not make contact, then it is not factored into the average values. There is a trend of generally decreasing the contact time as the Weber number is increased. Clearly the Weber number does not explain the entirety of the initial contact time as at lower Weber numbers some droplets lasted several milliseconds before contacting while others lasted only around one millisecond. As the Weber number is increased beyond around 25, it appears to become the dominant factor in the initial contact time of the droplet. Now it does appear that the vapor pressure is important for determining the initial contact time, as the lower vapor pressure values have noticeably larger initial contact times, and the acetone droplets have very low initial contact times independent of Weber number. The vapor pressure appears to relate to the initial contact time exponentially.

Number of Contact Locations

For the videos that captured droplets contacting the substrate, the number of individual contact initiation points was counted. This is a simple way to gain insight into the mechanism of the air film failure or droplet contact overall. An important note is that the ethanol droplets made contact in a visually messy manner, which made it impossible to count how many individual contact initiation points there were as the blobs of contact could have been multiple contact points that merged together. The frame rate used to capture the videos limited the accuracy of this data mainly for the ethanol droplets.

The number of contact points was counted manually, as identifying the contact points with an algorithm was too difficult with the variety of presentations of contact through the different impacts. The video of the droplet impact had to be paused and advanced frame-by-frame in order to count each individual contact point, as the contact points merge with each other and may only be separated from each for a single frame. Consider figure 4.30 below with example snapshots of one of the acetone droplet impacts.

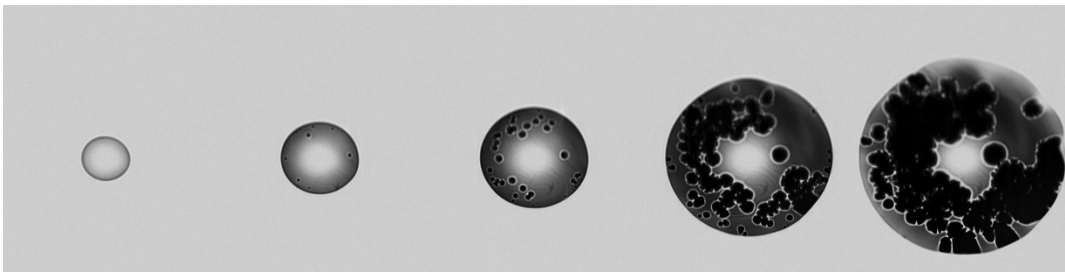


Figure 4.30 Typical contact progression for acetone droplets. Note, there is more than one frame of separation between the images, but these images are all from the same acetone droplet impact ($We = 25.9$).

The first image in figure 4.30 shows the droplet coming into view before any contact is made with the substrate. The second image already has several individual

contact locations, and with each successive image in the sequence more contact points are made. The last two images show the contact points merging, which is why the contact points in each frame of the video were counted to determine the total number of individual contact sites for that droplet impact. It is not possible to just examine the final frame of the impact and count all the contact points because they will have merged into one large contact area by then. Summary information for the number of contact points is depicted in figures 4.31 and 4.32 below.

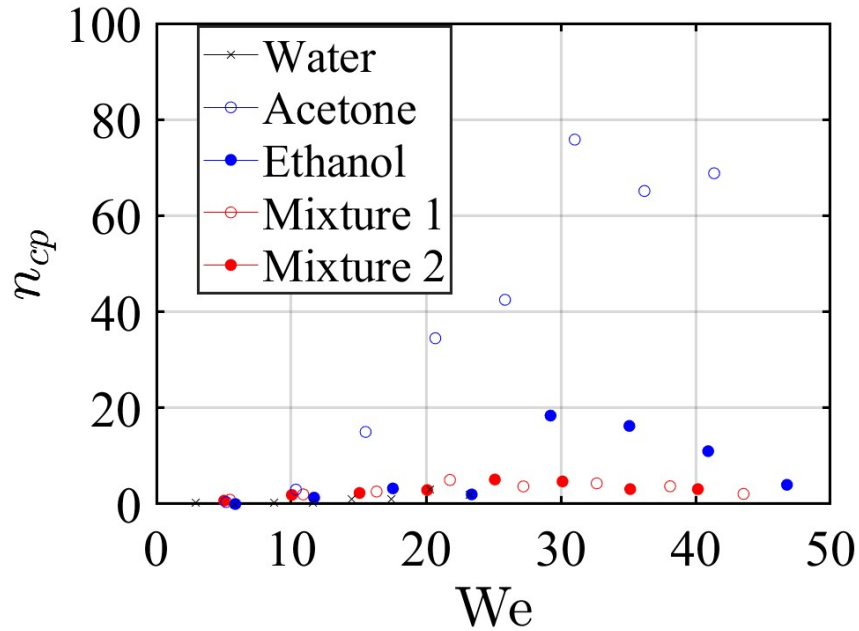


Figure 4.31 Number of contact points vs Weber number

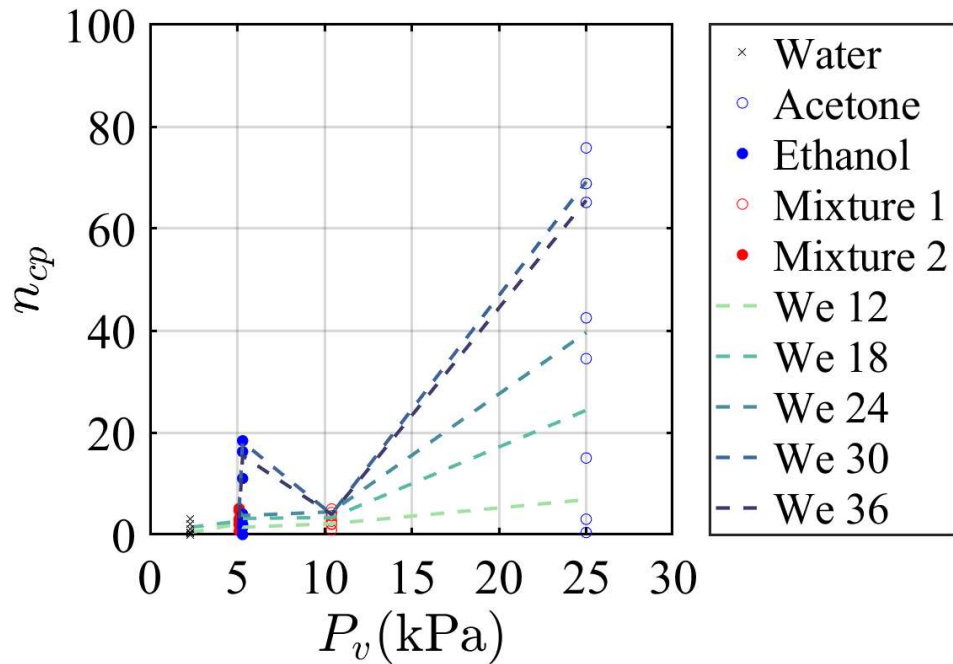


Figure 4.32 Number of contact points vs vapor pressure

These plots are of how many individual contact points were made throughout the contact process of the droplet compared to the Weber number and vapor pressure, respectively. The values were averaged for each group of parameters (release heights), and if there was no contact made then that experiment did not factor into the average value. In the Weber number plot, there does appear to be a region, around We 25 - 35, where there is an increased number of contact points, and then the number of contact points declines. There must also be another factor that is critical to determining the number of contact points as the acetone data points are all significantly higher than the other fluids. The Weber number alone is not enough to predict the number of contact points as the acetone droplets have on around an order of magnitude increase in number of contact points as compared to the other fluids. The number of contact points clearly increases with the vapor pressure for the pure fluids, but the two mixtures do not have a

similar increase. The two mixtures almost seem to have number of contact points being independent of the vapor pressure. There must be another variable at play with the mixtures. The mechanism allowing the significant increase in contact points must be suppressed in the mixtures.

Full Contact Time

Full contact was the time starting from when the droplet first came into view of TIRM and ending when the contact patch stopped expanding radially and filling in contact gaps under the droplet. Figure 4.33 below is an example image sequence of the ending stages of contact. As the contact points merge with each other and expand radially, they fill up the entire droplet's contact area. In the second image in the sequence, a faint gray line can be seen in the bottom left corner. That line is from the TIRM detecting the edge of the droplet, and once the contact has filled the area to that edge it slows down any movement significantly. This time is what is referred to herein as the full contact time. All of the full contact times are now analyzed below in figures 4.34 through 4.37.



Figure 4.33 Full contact identification (same acetone droplet video as figure 4.30 and note more than 1 frame of separation occurs between images)

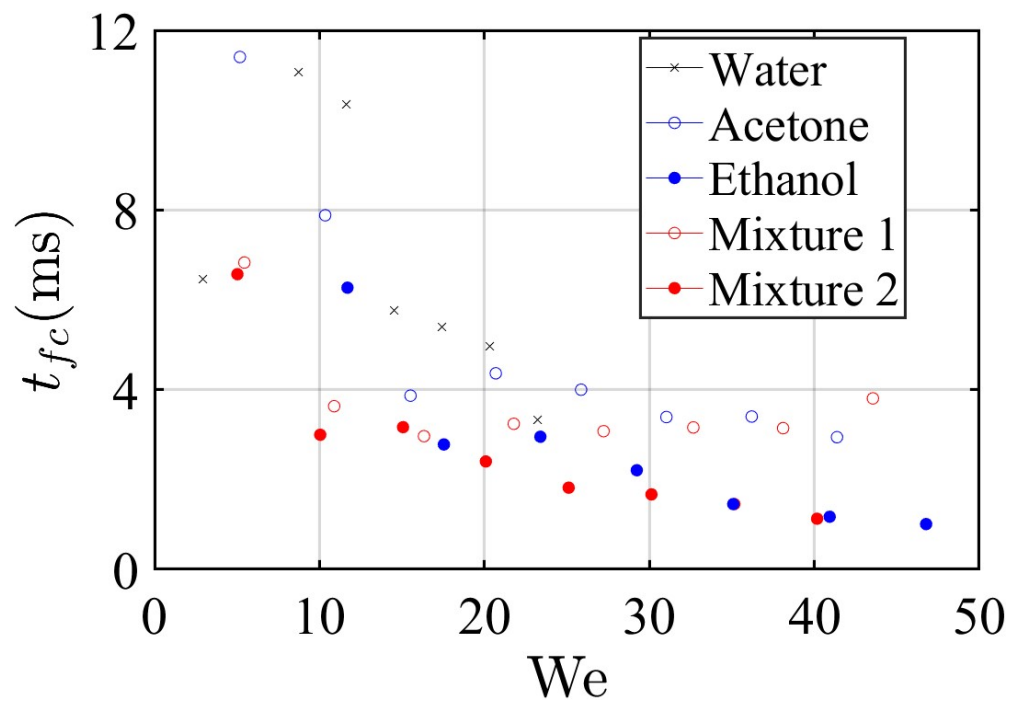


Figure 4.34 Weber number vs full contact time

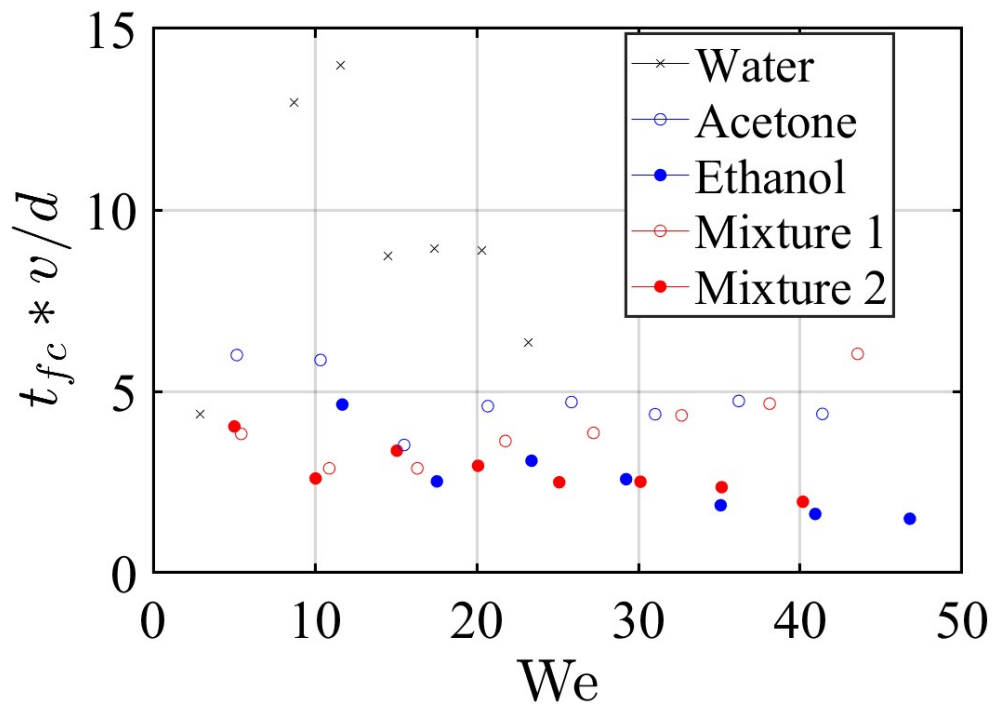


Figure 4.35 Weber number vs nondimensional full contact time

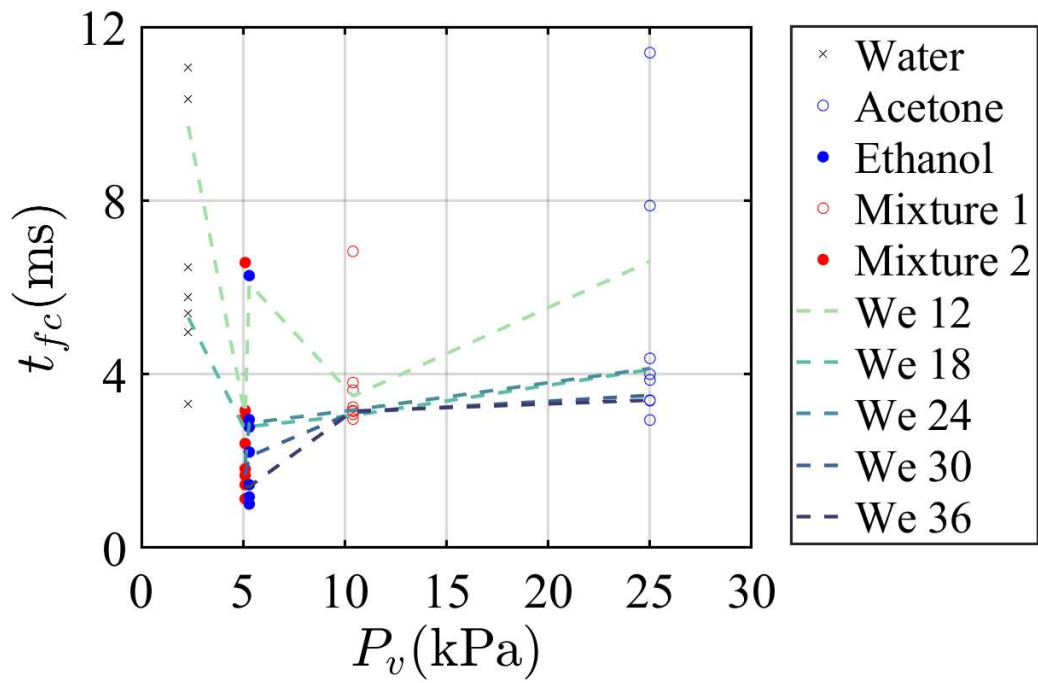


Figure 4.36 Vapor pressure vs full contact time

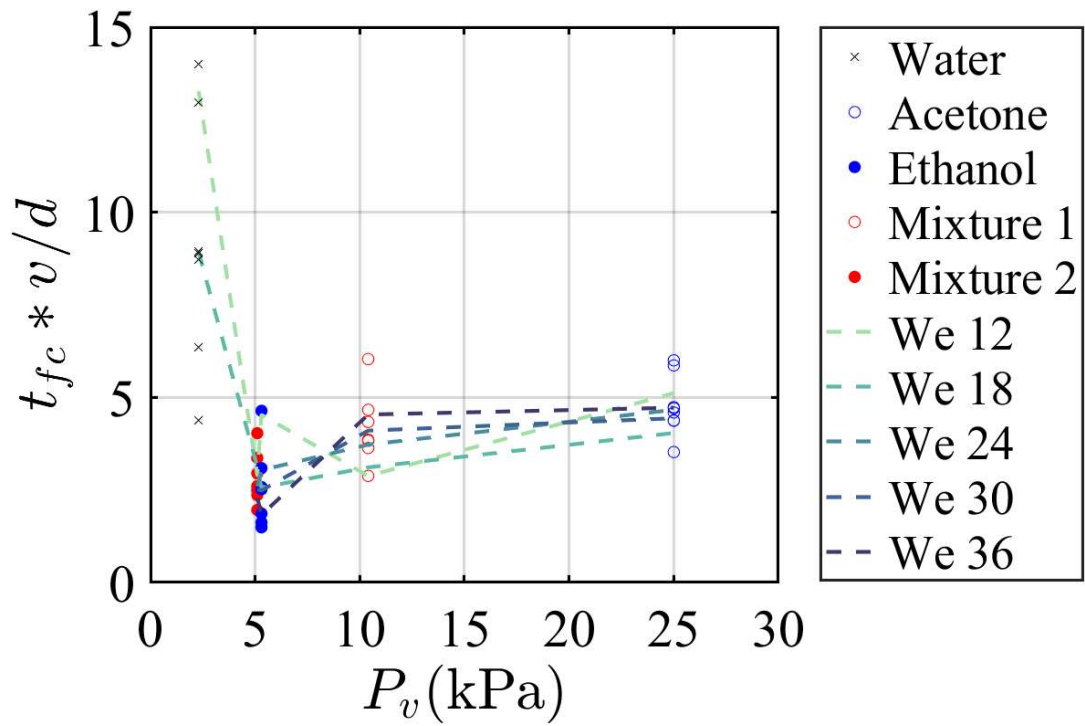


Figure 4.37 Vapor pressure vs nondimensional full contact time

The full contact time figures plot of all the data's initial contact time versus Weber number and vapor pressure, respectively. If the droplet did not make contact, then it is not factored into the average values. There is a trend of generally decreasing the full contact time as the Weber number is increased. These plots definitely indicate a more gradual transition of full contact time as the Weber number is increased. When the full contact time is non-dimensionalized by the inertial time scale, the We number nearly appears irrelevant to affecting the full contact time. It is also interesting to note that there is more variation in the full contact time of the different fluids at lower Weber numbers. That makes sense as the lower the Weber number the less important the kinetic energy is to the overall droplet behavior, which allows the vapor pressure to play a larger role in determining the full contact time. Interestingly, the full contact time does not appear to be affected by the vapor pressure, as the acetone droplets still took a relatively long time to make full contact. The vapor pressure does not seem to be as relevant of a factor for the full contact time as it was for the initial contact time. It is interesting to note that the shortest full contact times occurred for the ethanol and mixture 1 droplets. This may indicate that there is a specific region of vapor pressure that expedites the contact process of the droplets. Another viewpoint is that the mixture 2 and acetone droplets took longer to make full contact as the increased vapor pressure helped to suspend the droplets despite the air film rupturing already as the initial contact plot would indicate. To assess if the number of contact points was a lurking variable in predicting the full contact time, figure 4.38 below plots the number of contact points versus the dimensionless full contact time. The plot does not show any clear relationship between the number of contact points

and the dimensionless full contact time, however, so the number of contact points do not play a major role in the full contact time of droplet impacts.

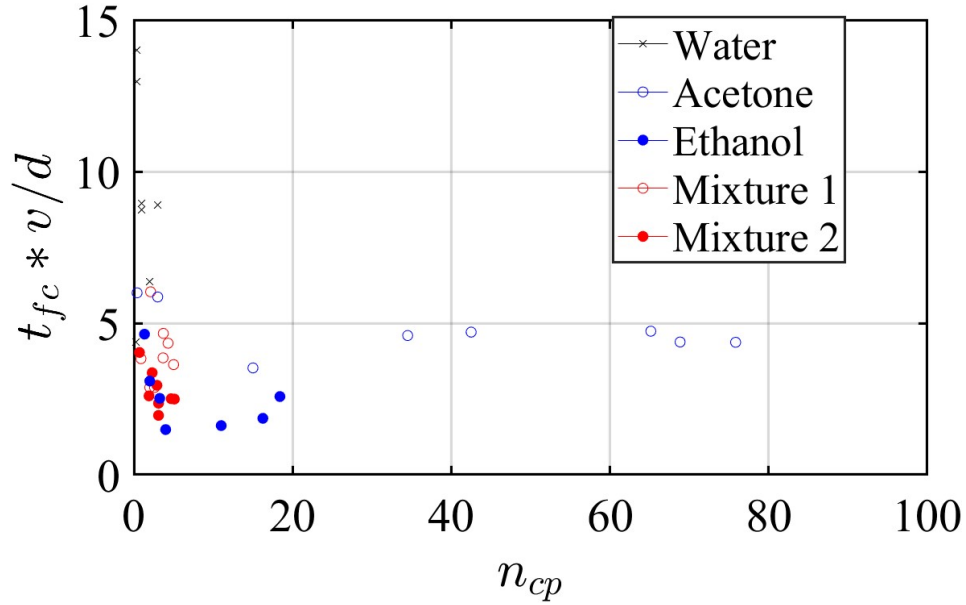


Figure 4.38 Number of contact points versus dimensionless full contact time

Contact Collapse Time

Contact collapse time is the difference in time between the initial and full contact times. Contact collapse time can alternatively be labeled the wetting time for the droplet impact. The equation relating the initial contact time, full contact time, and contact collapse time is listed in equation 4.1. Figures 4.39 through 4.43 plot the contact collapse time and its inertially non-dimensionalized version versus the Weber numbers and vapor pressures of each droplet impact, as well as the number of contact points.

$$t_{cc} = t_{fc} - t_c \quad (4.1)$$

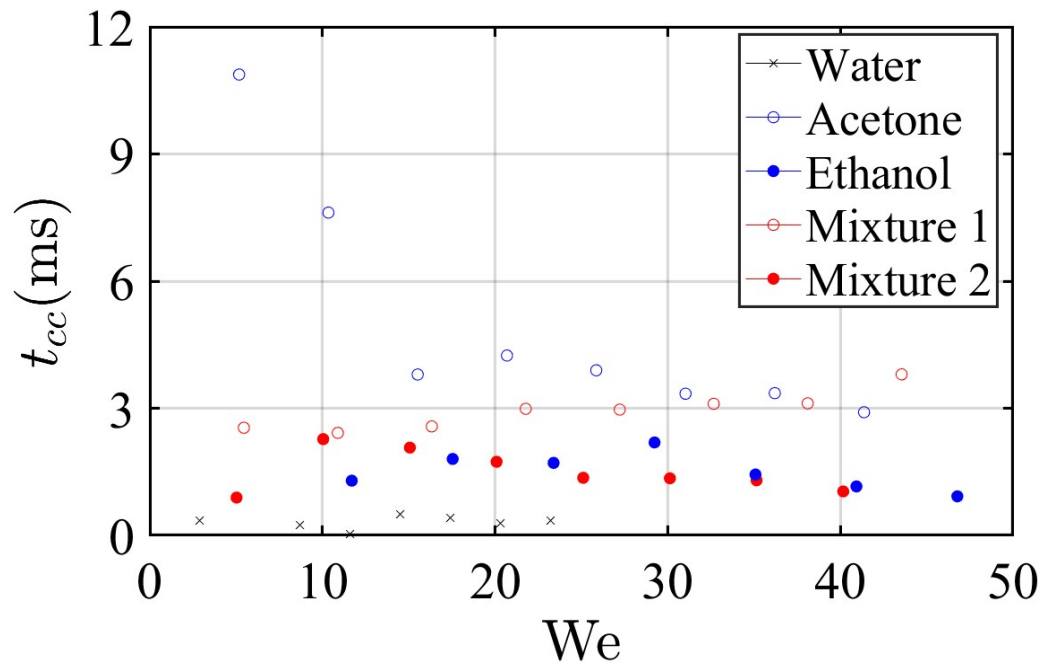


Figure 4.39 Contact collapse time versus Weber number

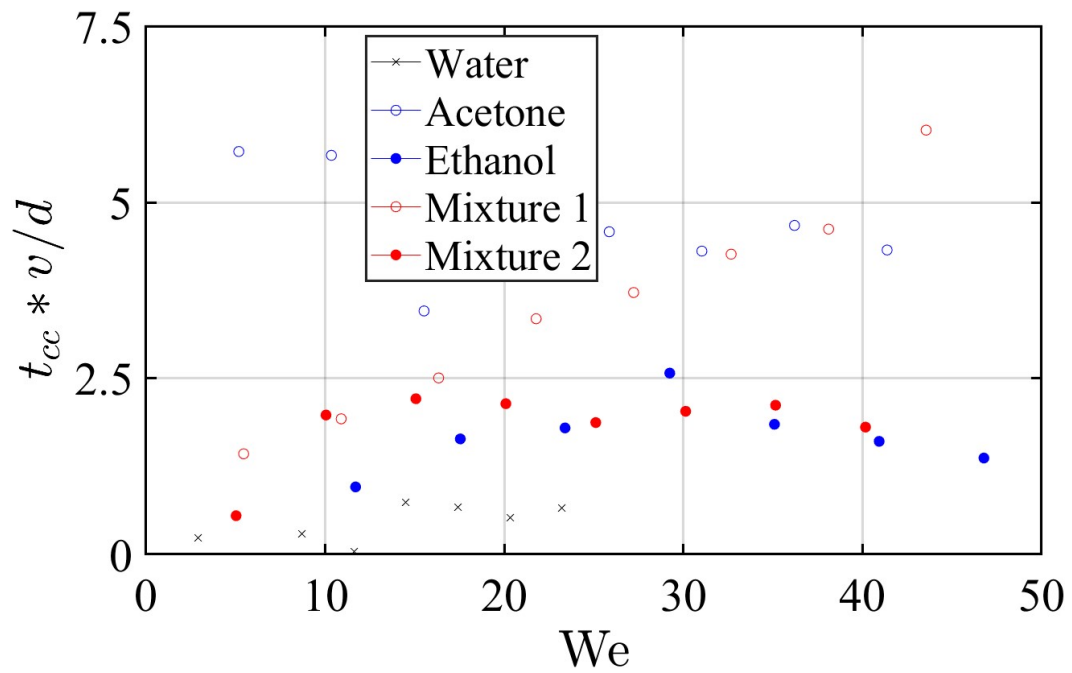


Figure 4.40 Dimensionless contact collapse time versus Weber number

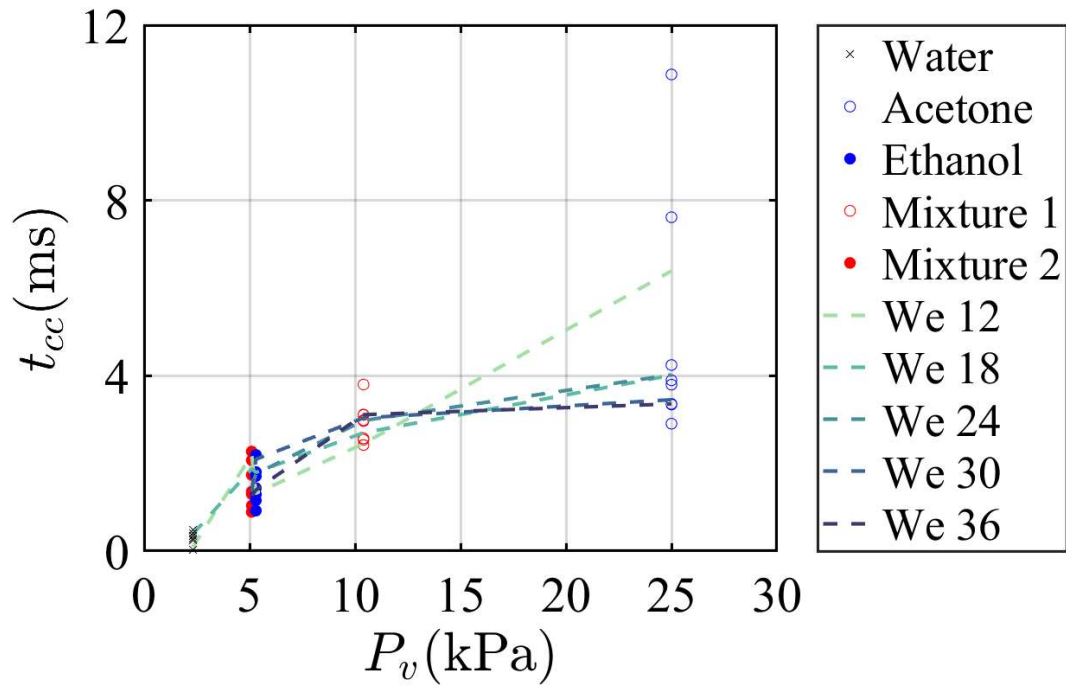


Figure 4.41 Contact collapse time versus vapor pressure

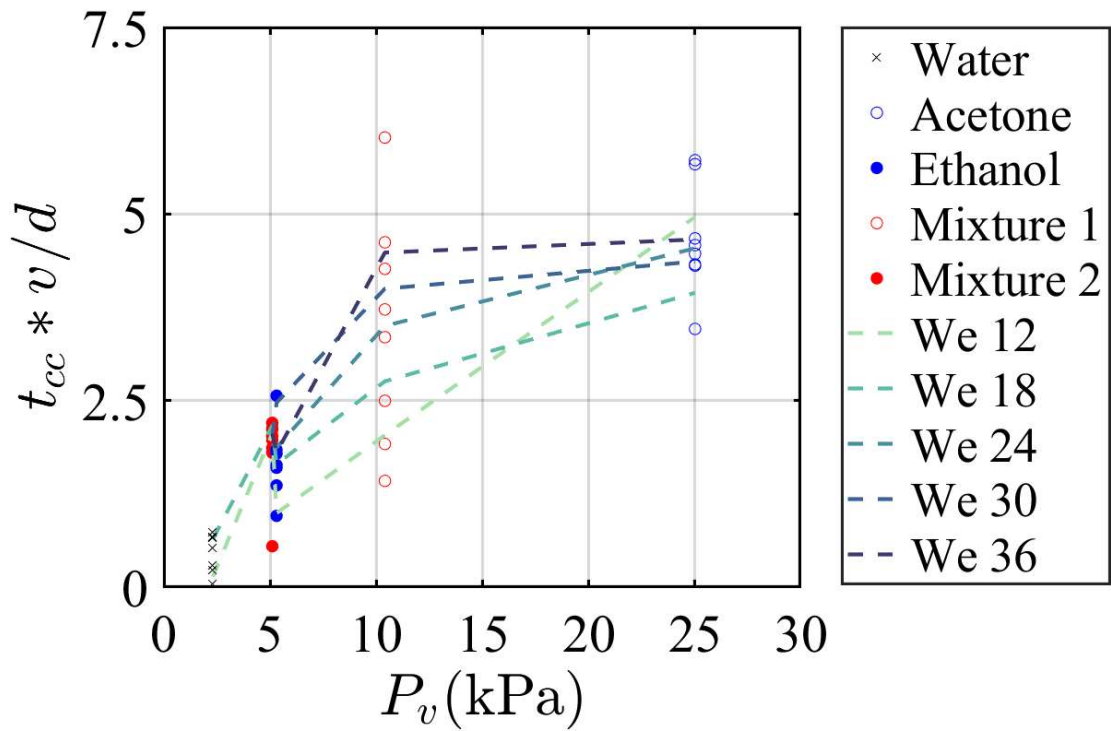


Figure 4.42 Dimensionless contact collapse time versus vapor pressure

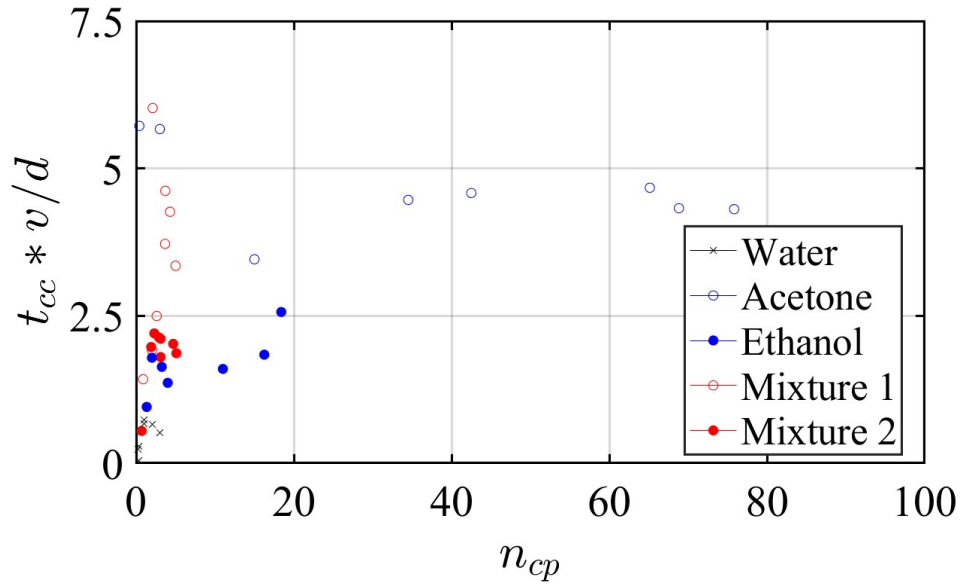


Figure 4.43 Number of contact points versus dimensionless contact collapse time

The contact collapse times convey a very similar lack of a relationship with the Weber number of the droplet impacts as the full contact times do. When the contact collapse times are non-dimensionalized by the inertial time scale, this lack of a relationship still holds true. The vapor pressure plots, however, have a noticeable relationship with the contact collapse times. As the vapor pressure increases, so does the contact collapse times. Perhaps the vapor outflow around the droplets does keep them aloft longer. Interestingly, from the constant Weber number contours on the vapor pressure vs contact collapse times, it appears that higher Weber numbers actually have longer contact collapse times. The number of contact points also does not appear to have a relationship with the contact collapse time, as the data shows no clear trends.

CHAPTER FIVE

Conclusions

Droplet impact experiments on a solid, lubricated substrate were performed to gain more insight into the mechanism of contact between the droplet and the substrate. The droplets were observed using TIRM to both view the droplets from the bottom and visualize features smaller than the microscale. Multiple fluids were used to vary the fluid parameters within the droplets themselves, and as a result, the vapor pressure has been shown to influence the contact dynamics of droplet impacts on solid substrates. As the vapor pressure increases, the droplets contact the substrate faster for the same We number (initial contact time). The number of individual contact points and contact collapse or wetting time both increase as the vapor pressure of the droplet increases.

The main application space for this research is spray coatings. The goal being to tune the spray to make full contact with the substrate faster and thus be more likely to adhere to the substrate as desired. A new question that formed from this research is how mixtures change the vapor pressure effect on the contact of the droplet. The two mixtures of water and acetone studied here have resisted the trends otherwise present in the data. On one hand they had low numbers of contact points and on the other hand they had the fastest full contact times. It was presumed that the number of contact points and the full contact time would be inversely related. Furthermore, it is not uncommon for spray coatings to be polymers or mixtures of multiple fluids.

Future Work

There are two main branches of future work for this research. The first branch consists of using more fluids to allow more data points for the vapor pressure effect between the values of vapor pressure for water and acetone. Perhaps the results were specific to acetone and ethanol and other fluids with similar vapor pressures would behave differently. The second branch would probe deeper into how the vapor pressure impacts various mixtures specifically.

APPENDIX

APPENDIX A

MATLAB Codes

TIRM Validation Code

```
%%%%%%%%%%%%%%%%%%%%%%%%%%%%%%%%%%%%%%%%%%%%%%%%%%%%%%%%%%%%%%%%%%%%%%%%%
%%%%%%%%%%%%%%%%%%%%%%%%%%%%%%%%%%%%%%%%%%%%%%%%%%%%%%%%%%%%%%%%%%%%%%%%%
% Clear Previous Data
clearvars, close all, clc
tic

%%%%%%%%%%%%%%%%%%%%%%%%%%%%%%%%%%%%%%%%%%%%%%%%%%%%%%%%%%%%%%%%%%%%%%%%%
%%%%%%%%%%%%%%%%%%%%%%%%%%%%%%%%%%%%%%%%%%%%%%%%%%%%%%%%%%%%%%%%%%%%%%%%%
% File Information

% Basic Data Information
set(0,'DefaultFigureWindowSize','docked')
                                % make figures open docked by
default
path = 'filepath_to_data';
                                % file path to folder with data
files = dir(strcat(path,'\*.tif'));
                                % structure array of file
information
ni = length(files);            % number of images

% Memory Allocation
I = cell(1,ni);                % image cell array memory
allocation
Mi = zeros(1,ni);              % max intensity in image
mi = zeros(1,ni);              % minimum intensity in image
sI = zeros(3,ni);              % size of images memory allocation
```

```

sizeI = zeros(1,ni);      % smaller length (row or column)
cI = cell(1,ni);         % cropped image array memory
allocation
cIt = cell(1,ni);        % cropped thresholded image array
memory allocation
zcI = cell(1,ni);        % zoomed cropped thresholded image
array mem alloc
GT = cell(1,ni);         % gap thickness memory allocation
cGT = cell(1,ni);        % gap thickness centered memory
allocation
clGT = cell(1,ni);       % same as cGT but with center lines
biti = 2^12-1;           % maximum intensity in image
phiinc = zeros(1,ni);    % incident angle array memory
allocation
FE = zeros(1,ni);        % major-minor diameter ratio memory
allocation
rot = zeros(1,ni);       % horizontal prism rotation memory
allocation

%%%%%%%%%%%%%%%%%%%%%%%%%%%%%%%%%%%%%%%%%%%%%%%%%%%%%%%%%%%%%%%%%%%%%%%%
%%%%%%%%%%%%%%%%%%%%%%%%%%%%%%%%%%%%%%%%%%%%%%%%%%%%%%%%%%%%%%%%%%%%%%%%
% Basic Optics Information

nprism = 1.5154;          % refractive index of prism
nair = 1;                 % refractive index of air
nlens = 1.5154;          % refractive index of lens

%%%%%%%%%%%%%%%%%%%%%%%%%%%%%%%%%%%%%%%%%%%%%%%%%%%%%%%%%%%%%%%%%%%%%%%%
%%%%%%%%%%%%%%%%%%%%%%%%%%%%%%%%%%%%%%%%%%%%%%%%%%%%%%%%%%%%%%%%%%%%%%%%
% Incident Angle Distortion Reference

% Calculate Incident Angles for Optics Setup
N1 = nprism/nair;         % ratio of refractive indices prism/air
ns = 10^5;               % number of values plotted
phi = linspace(30,90,ns);
                        % angle of incidence vector in degrees

```



```

phi4 = phi;           % angle of reflected light off top of
prism relative

                        % to plane normal to top surface
phi5 = phi-45;        % angle of reflected light off left
side of prism

                        % relative to plane normal to left
surface
phi6 = asind(N1.*(sind(phi5)));
                        % angle of refracted light off left
side of prism

                        % relative to plane normal to left
surface
F1 = real(cosd(phi4)./cosd(phi5).*cosd(phi6));
                        % optical transfer function - ratio of
width and height

                        % of a circle imaged on top of the
prism

%%%%%%%%%%%%%%%%%%%%%%%%%%%%%%%%%%%%%%%%%%%%%%%%%%%%%%%%%%%%%%%%%%%%%%%%
%%%%%%%%%%%%%%%%%%%%%%%%%%%%%%%%%%%%%%%%%%%%%%%%%%%%%%%%%%%%%%%%%%%%%%%%
% Loop Through All Files
for i = 1:ni

    % Create Image Files From All Files
    FILENAME = strcat(files(i).folder,'\ ',files(i).name);
    I[17] = imread(FILENAME);

%%%%%%%%%%%%%%%%%%%%%%%%%%%%%%%%%%%%%%%%%%%%%%%%%%%%%%%%%%%%%%%%%%%%%%%%
%%%%%%%%%%%%%%%%%%%%%%%%%%%%%%%%%%%%%%%%%%%%%%%%%%%%%%%%%%%%%%%%%%%%%%%%
% Gather Basic Info and Scale Data
    % Data for Image
    [sI(1,i),sI(2,i),sI(3,i)] = size(I{i});
                                % data rows and columns

    % Convert to Gray Scale
    if sI(3,i) == 3

```

```

        I{i} = rgb2gray(I{i}); % convert image file to
        grayscale
    end

    % Scale Intensities
    I{i} = double(I{i});      % convert data type to
    double
    I{i} = I{i}/biti;        % scale data by bit depth
    of image

%     % Plot Intensity Distributions
%     [Pixel,Bin] = imhist(I{i},biti);
%     figure
%     bar(Pixel);
%     axis([0 biti 0 200])
%     title(files(i).name)
%     xlabel('Intensity Values')
%     ylabel('Number of Pixels')

% Normalize Data
Mi(1,i) = max(max(I{i})); % max intensity
mi(1,i) = min(min(I{i})); % min intensity
I{i} = I{i}/Mi(1,i);      % normalized data

%%%%%%%%%%%%%%%%%%%%%%%%%%%%%%%%%%%%%%%%%%%%%%%%%%%%%%%%%%%%%%%%%%%%%%%%
%%%%%%%%%%%%%%%%%%%%%%%%%%%%%%%%%%%%%%%%%%%%%%%%%%%%%%%%%%%%%%%%%%%%%%%%
% Find Lenses in Images

% Divide Images in Interrogation Areas
r = 5; % interrogation area number of rows
and columns

% relative to the min total row and
columns (2/r)
NIA = (r-2)^2; % number of interrogation areas to
check

```

```

                                % note that r must be a whole
number to work
    IAc = sI(2,i)/r;    % number of columns of pixels in
one IA
    IAr = sI(1,i)/r;    % number of rows of pixels in one
IA

    % Loop Through IA's to Find Lens
    ai = round(IAc*3/2);    % center column of top left IA
of interest
    bi = round(IAr*3/2);    % center row of top left IA of
interest
    hi = zeros(1,NIA);    % memory allocation for
horizontal increment
    vi = zeros(1,NIA);    % memory allocation for
vertical increment
    mIIA = zeros(1,NIA);    % mean intensity of IA memory
allocation
    for j = 1:sqrt(NIA)
        hi(1,1+(j-1)*sqrt(NIA):3+(j-1)*sqrt(NIA)) =
0:sqrt(NIA)-1;
                                % horizontal increment
    end
    for j = 1:NIA            % loop through center IA's
        vi(1,j) = floor((j-1)/sqrt(NIA));
                                % vertical increment
        a = hi(1,j)*IAc+ai; % horizontal center of
interrogation area
        b = vi(1,j)*IAr+bi; % vertical center of
interrogation area

    % Index References of Interrogation Areas
    cm = round(a);          % center column
    cn = round(b);          % center row
    cl = ceil(cm-IAc/2);    % left cutoff
    cr = floor(cm+IAc/2);    % right cutoff

```

```

        ct = ceil(cn-IAr/2);    % top cutoff
        cb = floor(cn+IAr/2);  % bottom cutoff

        % Find Lens Location
        mIIA(1,j) = mean(mean(I{i}(ct:cb,cl:cr)));
    end
    [~,ind] = min(mIIA);        % find IA with minimum
    average intensity
    a = hi(1,ind)*IAC+ai;      % IA column
    b = vi(1,ind)*IAR+bi;      % IA row

    % Index References of Interrogation Areas
    cm = round(a);             % center column
    cn = round(b);             % center row
    cl = ceil(cm-IAC/2);       % left cutoff
    cr = floor(cm+IAC/2);      % right cutoff
    ct = ceil(cn-IAR/2);       % top cutoff
    cb = floor(cn+IAR/2);      % bottom cutoff

    % Remove Extra Pixel Info
    for k = ct:cb              % row index of base image
        for j = cl:cr          % column index of base
image
            cI{i}(k-(ct-1),j-(cl-1)) = I{i}(k,j);
                                % cropped image array
        end
    end

    % Check Interrogation Area Selection
    figure
    imshow(cI{i})
    title(files(i).name)

%%%%%%%%%%%%%%%%%%%%%%%%%%%%%%%%%%%%%%%%%%%%%%%%%%%%%%%%%%%%%%%%%%%%%%%%%%%%%%
%%%%%%%%%%%%%%%%%%%%%%%%%%%%%%%%%%%%%%%%%%%%%%%%%%%%%%%%%%%%%%%%%%%%%%%%%%%%%%
% Find Incident Angle

```

```

    for L = 1:2                                % To correct when lens on
IA border

        % Threshold Image
        [val,~] = min(min(cI{i}));
        minI = val;                            % minimum intensity used
        [val,~] = max(max(cI{i}));
        maxI = val;                            % minimum intensity used
        threshold = 0.5*(maxI+minI);
                                                % threshold intensity used

        % Make Image Binary (Inverted Intensity)
        [r,c] = size(cI{i});    % size of cropped image
        for j = 1:r
            for k = 1:c
                if cI{i}(j,k) < threshold
                    cIt{i}(j,k) = 1;
                else
                    cIt{i}(j,k) = 0;
                end
            end
        end

        % Fill Reflection Holes
        cIt{i} = imfill(cIt{i},'holes');
        cIp =
regionprops(cIt{i},'Orientation','MajorAxisLength',...
            'MinorAxisLength','Centroid');
                                                % cropped image lens shape
properties
    ang = cIp.Orientation;    % rotation angle of
diameters to axes
    MD = cIp.MajorAxisLength;
                                                % major diameter length
    mD = cIp.MinorAxisLength;

```

```

        % minor diameter length
        cen = cIp.Centroid;    % centroid location

    % Check Binary Image
    figure
    imshow(cIt{i})

    % Roughly Center Image
    rows(1,L) = round(cen(1,2)-r/2);
    cols(1,L) = round(cen(1,1)-c/2);
    rs = sum(rows); cs = sum(cols);
    for k = ct+rs:cb+rs
        for j = cl+cs:cr+cs
            cI{i}(k-(ct+rs-1),j-(cl+cs-1)) = I{i}(k,j);
        end
    end

    % Check Centered Binary Images
    figure
    imshow(cI{i})
end

% Find Incident Angle
FE(1,i) = mD/MD;    % major and minor diameter
ratio
[~,phii] = min(abs(FE(1,i)-F1));
                    % phi index
    phiinc(1,i) = phi(phii);    % angle of incidence onto
top of prism

                                % in degrees from normal
    rot(1,i) = ang;    % rotation of prism about
real vertical axis
%    phiinc = 45;    % angle of incidence in
degrees
%    resphi(1,i) = phim-phiinc;    % residual in measured
and expected angle

```

```

%%%%%%%%%%%%%%%%%%%%%%%%%%%%%%%%%%%%%%%%%%%%%%%%%%%%%%%%%%%%%%%%%%%%%%%%
%%%%%%%%%%%%%%%%%%%%%%%%%%%%%%%%%%%%%%%%%%%%%%%%%%%%%%%%%%%%%%%%%%%%%%%%
% Correct Incident Angle Distortion and Rotation of Prism

% Rotate Image
I{i} = imrotate(I{i},ang);

% Resize Image
r = round(SI(1,i)/FE(1,i));      % new number or rows in
image
c = round(SI(2,i));              % new number of columns
in image
I{i} = imresize(I{i},[r,c]);    % resizes image

%      % Check Corrected Image
%      figure
%      imshow(I{i})

% Zoom In
leng = round(MD*2.5);            % length of zoomed-in
width and height
for j = 1:leng
    for k = 1:leng
        zcI{i}(j,k) = I{i}(round(j+(cn+rs)/FE(1,i)-
leng/2),...
                                round(k+cm+cs-leng/2));
    end
end

% Check Zoomed-In Corrected Image
figure
imshow(zcI{i})
title(files(i).name)

%%%%%%%%%%%%%%%%%%%%%%%%%%%%%%%%%%%%%%%%%%%%%%%%%%%%%%%%%%%%%%%%%%%%%%%%
%%%%%%%%%%%%%%%%%%%%%%%%%%%%%%%%%%%%%%%%%%%%%%%%%%%%%%%%%%%%%%%%%%%%%%%%

```

```

%%%%%%%%%%%%%%%%%%%%%%%%%%%%%%%%%%%%%%%%%%%%%%%%%%%%%%%%%%%%%%%%%%%%%%%%
% Intensity to Gap Thickness Mapping

% Generate Variables
ys = 1500*10^-9;          % y axis limit used
d = linspace(0,ys,ns);    % gap thickness vector in
meters
iu = sqrt(-1);            % imaginary unit
lambda = 636.2305908*10^-9;
                           % wavelength of light used
(100% intensity)

% Angles
phi1 = phiinc(1,i);       % rewriting angle of incidence
from my
                           % notation to shirota's
notation (degrees)
phi2 = asind(nprism/nair*sind(phi1));
                           % angle 2 snell's law
refraction relation
phi3 = asind(nair/nlens*sind(phi2));
                           % angle 3 snell's law
refraction relation

% Reflection Coefficients
r12s = (nprism*cosd(phi1)-nair*cosd(phi2))./(...
        (nprism*cosd(phi1)+nair*cosd(phi2)));
                           % light reflected at 1-2 boundary
from the 1 side
                           % back to the 1 side for s
polarized light
r32s = (nlens*cosd(phi3)-nair*cosd(phi2))./(...
        (nlens*cosd(phi3)+nair*cosd(phi2)));
                           % light reflected at 3-2 boundary
from the 3 side
                           % back to the 3 side for s

```



```

polarized light
    r12p = (nair*cosd(phi1)-nprism*cosd(phi2))./...
            (nair*cosd(phi1)+nprism*cosd(phi2));
                                % light reflected at 1-2
boundary from the 1
                                % side back to the 1 side for p
polarized light
    r32p = (nair*cosd(phi3)-nlens*cosd(phi2))./...
            (nair*cosd(phi3)+nlens*cosd(phi2));
                                % light reflected at 3-2
boundary from the 3
                                % side back to the 3 side for p
polarized light

    % Rewrite Based on Stokes' Relations
    r23s = -r32s;
    r23p = -r32p;

    % Path Difference
    delta = 4*pi*d/lambda.*(nair^2-
nprism^2*(sind(phi1)).^2).^^(1/2);

    % Main Equation (Eqn 5)
    RS =
(r12s+r23s.*exp(iu*delta))./(1+r12s.*r23s.*exp(iu*delta));
                                % reflectance coefficient s
polarized light
    Rp =
(r12p+r23p.*exp(iu*delta))./(1+r12p.*r23p.*exp(iu*delta));
                                % reflectance coefficient p
polarized light

    Rsp = abs(Rs.^2);           % normalized reflection
intensity s polarized
                                % light as shirota used in fig
6

```

```

        Rpp = abs(Rp.^2);           % normalized reflection
intensity p polarized
                                     % light as shirota used in fig
6

% Organize Information
RIs = [d;Rsp];
RIp = [d;Rpp];

% Plot Results
figure
hold on
plot(RIs(2,:),RIs(1,:), 'r.', 'MarkerSize',0.5)
plot(RIp(2,:),RIp(1,:), 'b.', 'MarkerSize',0.5)
hold off
grid on
xlabel('Normalized Reflection Intensity |r^2|')
ylabel('Gap Thickness (m)')
title(files(i).name)
axis([0,1,0,2*ys/3])

%%%%%%%%%%%%%%%%%%%%%%%%%%%%%%%%%%%%%%%%%%%%%%%%%%%%%%%%%%%%%%%%%%%%%%%%
%%%%%%%%%%%%%%%%%%%%%%%%%%%%%%%%%%%%%%%%%%%%%%%%%%%%%%%%%%%%%%%%%%%%%%%%
% Convert Intensity to Gap Thickness

    for j = 1:leng
        for k = 1:leng
            [~,index] = min(abs(RIp(2,:)-zcI{i}(j,k)));
                                     % rIp since we use p polarized
light
            zGT{i}(j,k) = RIp(1,index);
                                     % Gap Thickness cell array of image
i

        end
    end
end

```

```

        for j = 1:r
            for k = 1:c
                [~,index] = min(abs(RIp(2,:)-I{i}(j,k)));
                                % rIp since we use p polarized
light
                GT{i}(j,k) = RIp(1,index);
                                % Gap Thickness cell array of image
i
            end
        end

% Plot Results
figure
surf(zGT{i},'linestyle','none');
title(files(i).name)
xlabel('columns')
ylabel('rows')
zlabel('Gap Thickness (m)')
colormap jet
colorbar
%     view([0,90])

%%%%%%%%%%%%%%%%%%%%%%%%%%%%%%%%%%%%%%%%%%%%%%%%%%%%%%%%%%%%%%%%%%%%%%%%%%%%%%
%%%%%%%%%%%%%%%%%%%%%%%%%%%%%%%%%%%%%%%%%%%%%%%%%%%%%%%%%%%%%%%%%%%%%%%%%%%%%%
% Center Lens in its Interrogation Area

% Lens Focal Length from Filename
lnf = length(files(i).name);
                                % number of characters in
filename
    FL = zeros(1,lnf);          % focal length vector mem alloc
    for j = 1:lnf
        FL(1,j) = str2double(files(i).name(j));
    end
    j = 1;
    while isnan(FL(1,j))

```

```

        j = j+1;
    end
    k = j;
    while ~isnan(FL(1,k))
        k = k+1;
    end
    k = k-1;
    p = 1;
    for L = j:k
        aFL(1,p) = num2str(FL(1,L));
        p = p+1;
    end
    aFL = strcat(aFL); aFL = str2double(aFL);

    % Actual Lens Radius
    NP = 79; ND = 0.000312; % needle diameter in pixels and
m
    PpL = NP/ND;           % pixels per m
    LpP = ND/NP;           % meters per pixel
    R = aFL*(nlens-1)/1000; % radius of curvature of lens
in m
    Rp = R*PpL;           % radius of curvature of lens
in pixels

    for P = 1:2
        % Generate Surface Fit
        if P == 1
            cent = round(leng/2);
            row = round(cent-
0.2*leng):round(cent+0.2*leng);
            col = round(cent-
0.2*leng):round(cent+0.2*leng);
        else
            cent = round(cleng/2);
            row = round(cent-
0.45*cleng):round(cent+0.45*cleng);

```

```

        col = round(cent-
0.45*cleng):round(cent+0.45*cleng);
    end
    r = size(row,2); c = size(col,2);
    x = zeros(r*c,1); y = zeros(r*c,1); z =
zeros(r*c,1);

                                                    % memory allocation
    num = 1;                                     % counting variable
    for j = row
        for k = col
            if P == 1
                if zGT{i}(j,k) >
0.5*(max(max(zGT{i})))...
-
min(min(zGT{i}))) + min(min(zGT{i}))
                    else
                        x(num,1) = (k-cent)*LpP;
                        y(num,1) = (j-cent)*LpP;
                        z(num,1) = zGT{i}(j,k);
                        num = num+1;
                    end
                else
                    if czGT{i}(j,k) >
0.5*(max(max(czGT{i})))...
-
min(min(czGT{i}))) + min(min(czGT{i}))
                        else
                            x(num,1) = (k-cent)*LpP;
                            y(num,1) = (j-cent)*LpP;
                            z(num,1) = czGT{i}(j,k);
                            num = num+1;
                        end
                    end
                end
            end
        end
    end
    fo = fitoptions('Method','NonlinearLeastSquares');

```

```

ft = fittype('-(d^2-(x-a)^2-(y-
b)^2)^(1/2)+c','independent',...

{'x','y'},'dependent','z','coefficients',{'a','b','c','d'},
...
    'options',fo);
[f,gof,other] =
fit([x,y],z,ft,'MaxFunEvals',50000,'MaxIter',50000,'TolFun'
,...
    10^-21,'TolX',10^-18,'DiffMaxChange',100,...
    'DiffMinChange',10^-
21,'StartPoint',[0,0,5*R,2*R],'Algorithm'...
    ,'Levenberg-Marquardt','Robust','LAR');

%           % Check Fit
%           figure
%           p = plot(f);
%           p.LineStyle = 'none';
%           colormap jet
%           colorbar
%           hold on
%           plot3(x,y,z,'k.')
%           title(files(i).name)
%           xlabel('columns (m)')
%           ylabel('rows (m)')
%           zlabel('Gap Thickness (m)')
%           plot3(f.a,f.b,(f.c-
f.d)*1.01,'r.','MarkerSize',30)
%           hold off
% %           view([0,90])
%           title(files(i).name)

% Adjust Image to Center
cleng = round(0.4*leng);           % center image side
length pixels
icen = round(leng/2-cleng/2);     % initial center

```

```

location
    sa(1,P) = f.a/LpP; sb(1,P) = f.b/LpP;
    ssa = sum(sa); ssb = sum(sb);
    for j = 1:cleng
        for k = 1:cleng
            if P == 1
                czGT{i}(j,k) =
zGT{i}(j+icen+round(ssb),...
                    k+icen+round(ssa));
                    % centered Gap Thickness
cell array
            else
                czGT{i}(j,k) =
zGT{i}(j+icen+round(ssb),...
                    k+icen+round(ssa));
                    % centered Gap Thickness
cell array
            end
        end
    end

    % Add Center Lines to Check Centering
    xc = floor(cleng/2); % center column
    yc = floor(cleng/2); % center row
    val = (max(max(czGT{i}))-min(min(czGT{i}))) / 2;
    for k = 1:cleng % loop through rows
        for j = 1:cleng % loop through columns
            if k == yc || j == xc
                % if row or column matches
center row or
                    % column value
                    clGT{i}(k,j) = val;
            else % remaining points
                clGT{i}(k,j) = czGT{i}(k,j);
            end
        end
    end
end

```

```

end

%      % Check Centered Images
%      figure
%      surf(c1GT{i},'linestyle','none');
%      title(files(i).name)
%      xlabel('columns')
%      ylabel('rows')
%      zlabel('Gap Thickness (m)')
%      view([0,90])
%      colormap jet
%      colorbar

end

sa = []; sb = [];      % clear the centering info

% Vertical Shift in Data
shp(1,i) = f.c-f.d;      % pixel shift of p data
czGT{i} = czGT{i}-shp(1,i);

% Check Fit
figure
p = plot(f);
p.LineStyle = 'none';
colormap jet
colorbar
hold on
plot3(x,y,z,'k.')
title(files(i).name)
xlabel('columns (m)')
ylabel('rows (m)')
zlabel('Gap Thickness (m)')
plot3(f.a,f.b,(f.c-f.d)*1.01,'r.','MarkerSize',30)
hold off
%      view([0,90])
title(files(i).name)

```



```

% Check Centered Images
figure
surf(cLGT{i},'linestyle','none');
title(files(i).name)
xlabel('columns')
ylabel('rows')
zlabel('Gap Thickness (m)')
view([0,90])
colormap jet
colorbar

%%%%%%%%%%%%%%%%%%%%%%%%%%%%%%%%%%%%%%%%%%%%%%%%%%%%%%%%%%%%%%%%%%%%%%%%
%%%%%%%%%%%%%%%%%%%%%%%%%%%%%%%%%%%%%%%%%%%%%%%%%%%%%%%%%%%%%%%%%%%%%%%%
% Building Radial Profiles

% Gap Thickness Centered Expansion
r = round(SI(1,i)/FE(1,i)); % new number or rows in
image
c = round(SI(2,i)); % new number of columns
in image
EL = 2.0*leng; % expanded length
icenr = round((cn+rs)/FE(1,i)-EL/2); % initial
center row location
icenc = round(cm+cs-EL/2); % initial center
column location
for j = 1:EL
    for k = 1:EL
        czLGT{i}(j,k) = GT{i}(j+icenr+round(ssb),...
            k+icenc+round(ssa));
    end
end

% Add Center Lines to Check Centering
xc = EL/2; yc = EL/2;% center point
% val = (max(max(czLGT{i}))-min(min(czLGT{i}))) / 2;
val = max(max(czLGT{i}));

```

```

    for k = 1:EL      % loop through rows
        for j = 1:EL  % loop through columns
            if k == yc || j == xc
                % if row or column matches center
row or
                % column value
                clGT{i}(k,j) = val;
            else      % remaining points
                clGT{i}(k,j) = czLGT{i}(k,j);
            end
        end
    end
end

% Check Expanded Centered Images
figure
surf(clGT{i},'linestyle','none');
title(files(i).name)
xlabel('columns')
ylabel('rows')
zlabel('Gap Thickness (m)')
view([0,90])
colormap jet
colorbar

% Data Profiles
ai = 1; da = 10; af = 360;

a = ai:da:af;      % angle vector parameters
r = round(2.00*mD); % angle vector
as = length(a);    % pixel radius used
ip = zeros(as,r);  % length of angles vector
                    % memory allocation

for j = 1:as
    xf = xc+round(r*cosd(a(j)));
    % final x coordinate point
    yf = yc+round(r*sind(a(j)));

```

```

                                % final y coordinate point
    xe = [xc,xf]; % x endpoints
    ye = [yc,yf]; % y endpoints
    ip(j,:) = improfile(czLGT{i},xe,ye,r);
end
ips = mean(ip); % average profiles

% Actual Lens Profiles
xc = 0; yc = 0; % calibration of center of
circle
a = 0; b = yc+(R^2-xc^2)^(1/2);
                                % circle equation center shift
parameters
xi = 0; nx = 1000; xf = r*LpP;
                                % x vector parameters
x = linspace(xi,xf,nx); % "x" vector of lens profile
y = b-(R^2-(x-a).^2).^(1/2);
                                % "y" vector of lens profile
xd = 1:length(ips); % vector for plotting in pixels
xd = xd-1; % start at zero
xd = xd*LpP; % vector for plotting in m

% Lens Profile to Data Comparison
figure
hold on
plot(x,y)
plot(xd,ips,'.')
hold off
legend('Theoretical Profile','Data
Profile','Location','NorthWest')
title(files(i).name)
xlabel('Radius From Center (m)')
ylabel('Gap Thickness (m)')

% Residuals Plot
for j = 1:length(xd)

```

```

        [~,p] = min(abs(xd(j)-x));
        res(1,j) = ips(j)-y(p);
    end
    figure
    hold on
    plot(xd,zeros(1,length(xd)))
    plot(xd,res,'r.')
    hold off
    grid on
    title('Residuals')
    xlabel('Radius (m)')
    ylabel('Gap Thickness Difference (m)')
    res = [];

%%%%%%%%%%%%%%%%%%%%%%%%%%%%%%%%%%%%%%%%%%%%%%%%%%%%%%%%%%%%%%%%%%%%%%%%%%%%%%
%%%%%%%%%%%%%%%%%%%%%%%%%%%%%%%%%%%%%%%%%%%%%%%%%%%%%%%%%%%%%%%%%%%%%%%%%%%%%%
% Uncertainty of Data

end

table(phiinc',rot',shp','VariableNames',{'Incident Angle
(deg)'}...
    'Rotation Angle (deg)','Vertical Data Shift (m)'})

toc

```

Drop Size Code

```

%%%%%%%%%%%%%%%%%%%%%%%%%%%%%%%%%%%%%%%%%%%%%%%%%%%%%%%%%%%%%%%%%%%%%%%%%%%%%%
%%%%%%%%%%%%%%%%%%%%%%%%%%%%%%%%%%%%%%%%%%%%%%%%%%%%%%%%%%%%%%%%%%%%%%%%%%%%%%
% Clear Current Information
clearvars,close all,clc

%%%%%%%%%%%%%%%%%%%%%%%%%%%%%%%%%%%%%%%%%%%%%%%%%%%%%%%%%%%%%%%%%%%%%%%%%%%%%%
%%%%%%%%%%%%%%%%%%%%%%%%%%%%%%%%%%%%%%%%%%%%%%%%%%%%%%%%%%%%%%%%%%%%%%%%%%%%%%

```

```

% Start Timer of Code
tic

%%%%%%%%%%%%%%%%%%%%%%%%%%%%%%%%%%%%%%%%%%%%%%%%%%%%%%%%%%%%%%%%%%%%%%%%
%%%%%%%%%%%%%%%%%%%%%%%%%%%%%%%%%%%%%%%%%%%%%%%%%%%%%%%%%%%%%%%%%%%%%%%%
% File Information
set(0,'DefaultFigureWindowSize','docked')
                                % make figures open docked by
default
path = 'filepath_to_data';
                                % file path to folder with data
files = dir(strcat(path,'\*.tif'));
                                % structure array of file
information
ni = length(files);            % number of images

%%%%%%%%%%%%%%%%%%%%%%%%%%%%%%%%%%%%%%%%%%%%%%%%%%%%%%%%%%%%%%%%%%%%%%%%
%%%%%%%%%%%%%%%%%%%%%%%%%%%%%%%%%%%%%%%%%%%%%%%%%%%%%%%%%%%%%%%%%%%%%%%%
% Memory Allocation
I = cell(1,ni);                % image cell array memory
allocation
sI = zeros(3,ni);              % size of images memeory allocation
sizeI = zeros(1,ni);           % smaller length (row or column)
Mi = zeros(1,ni);              % max intensity in image
mi = zeros(1,ni);              % minimum intensity in image

%%%%%%%%%%%%%%%%%%%%%%%%%%%%%%%%%%%%%%%%%%%%%%%%%%%%%%%%%%%%%%%%%%%%%%%%
%%%%%%%%%%%%%%%%%%%%%%%%%%%%%%%%%%%%%%%%%%%%%%%%%%%%%%%%%%%%%%%%%%%%%%%%
% Basic Image Information

% Loop Through All Files
for i = 1:ni

    % Create Array from Image Files
    FILENAME = strcat(files(i).folder,'\ ',files(i).name);
    I{i} = imread(FILENAME);    % image array

```

```

% Image File Info
[sI(1,i),sI(2,i),sI(3,i)] = size(I{i});
                                % data rows and columns

% Convert to Gray Scale
if sI(3,i) == 3
    I{i} = rgb2gray(I{i}); % convert image file to
grayscale
end

% Allow Math on Pixel Info
I{i} = double(I{i});          % convert data type to
double

% Allow im- commands
Mi(1,i) = max(max(I{i}));    % maximum pixel intensity
in image
mi(1,i) = min(min(I{i}));    % minimum pixel intensity
in image
I{i} = I{i}/Mi(1,i);

%      % Check Images
%      figure
%      imshow(I{i})
%      title(files(i).name)

%%%%%%%%%%%%%%%%%%%%%%%%%%%%%%%%%%%%%%%%%%%%%%%%%%%%%%%%%%%%%%%%%%%%%%%%
%%%%%%%%%%%%%%%%%%%%%%%%%%%%%%%%%%%%%%%%%%%%%%%%%%%%%%%%%%%%%%%%%%%%%%%%
% Threshold Images

% Intensity Distribution
bn = Mi(1,i);                % number of bins
[Pix,Bin] = imhist(I{i},bn); % intensity distribution
PT = sI(1,i)*sI(2,i)*0.005; % pixel threshold for peaks
[peaks] = find(Pix>PT);      % find peak regions

```

```

% Find Peak Edges
j = 0; k = 0; % counting variables
while j < length(peaks)-1
    j = j+1;
    if peaks(j+1)-peaks(j) > 10
        k = k+1;
        pe(k) = peaks(j); % peak edge values
        k = k+1;
        pe(k) = peaks(j+1);
    end
end
T = 0.95*pe(end)/Mi(1,i); % image threshold value
pe = [];

% Thresholding Process
I{i} = I{i} < T; % creates logical image
I{i} = double(I{i}); % convert back to double to
fill
    I{i} = imfill(I{i}); % fill in "bright" spots
from reflections
    I{i} = logical(I{i}); % convert back to logical
for regionprops

% Check Threshold
figure
imshow(I{i})
if files(i).name(1) == '1'
    title('Mixture 1');
elseif files(i).name(1) == '2'
    title('Mixture 2');
elseif files(i).name(1) == 'a'
    title('Acetone')
elseif files(i).name(1) == 'e'
    title('Ethanol')
elseif files(i).name(1) == 'w'

```

```

        title('water')
    end

%%%%%%%%%%%%%%%%%%%%%%%%%%%%%%%%%%%%%%%%%%%%%%%%%%%%%%%%%%%%%%%%%%%%%%%%%%%%%%
%%%%%%%%%%%%%%%%%%%%%%%%%%%%%%%%%%%%%%%%%%%%%%%%%%%%%%%%%%%%%%%%%%%%%%%%%%%%%%
% Droplet Geometry Information

% Main Command
DGI =
regionprops('table',I{i},'Area','Circularity','Eccentricity',
',...

'MajorAxisLength','MinorAxisLength','Orientation','Centroid
');

% Check Region Identified as Droplet
cen = DGI.Centroid;           % centroids of all regions
rad = (DGI.MajorAxisLength+DGI.MinorAxisLength)/4;
                                % average radius of each
region
[rad,ind] = max(rad);          % maximum radius found
cen = cen(ind,:);             % corresponding centroid
hold on
viscircles(cen,rad);          % circle visulaization
hold off

% Infomation of Importance
d(i,1) = round(rad*2);        % droplet diameter
A(i,1) = DGI.Area(ind);       % droplet cross-section
area
E(i,1) = DGI.Eccentricity(ind);
                                % droplet eccentricity
C(i,1) = DGI.Circularity(ind)^-1;
                                % droplet eccentricity

% Secondary Information

```



```

md(i,1) = DGI.MinorAxisLength(ind);
                                % minor diameter (for
needles)
end

%%%%%%%%%%%%%%%%%%%%%%%%%%%%%%%%%%%%%%%%%%%%%%%%%%%%%%%%%%%%%%%%%%%%%%%%
%%%%%%%%%%%%%%%%%%%%%%%%%%%%%%%%%%%%%%%%%%%%%%%%%%%%%%%%%%%%%%%%%%%%%%%%
% Scale Information
[ned] = find(md < 200);          % index of needle images
% ppm = md(ned)/0.312;          % pixels per millimeter
of image group
ppm = [118,120,119,119]/0.312; % pixels per millimeter of
image group

                                % manually measured with
ImageJ
L = length(ned);                % number of needle scale
bars
Ni(2:L+1) = ned(1:L);           % start needle index at
zero
k = 1;
for i = 1:L
    for j = Ni(i)+1:Ni(i+1)-1    % assumes needle image is
the last image
                                % in the corresponding
image sequence
        nd(k,1) = d(j,1)/ppm(i); rd(k,1) =
round(1000*nd(k,1))/1000;
                                % droplet diameter in
millimeters
        nA(k,1) = A(j,1)/ppm(i)^2; rA(k,1) =
round(1000*nA(k,1))/1000;
                                % droplet area in
millimeters
        nE(k,1) = E(j,1); rE(k,1) =
round(1000*nE(k,1))/1000;
        nC(k,1) = C(j,1); rC(k,1) =

```

```

round(1000*nc(k,1))/1000;

                                % ignoring needle images in
final table
    name{k,1} = files(j).name;
                                % file name array
    k = k+1;
end
end

%%%%%%%%%%%%%%%%%%%%%%%%%%%%%%%%%%%%%%%%%%%%%%%%%%%%%%%%%%%%%%%%%%%%%%%%%%%%%%
%%%%%%%%%%%%%%%%%%%%%%%%%%%%%%%%%%%%%%%%%%%%%%%%%%%%%%%%%%%%%%%%%%%%%%%%%%%%%%
% Statistics
m = 1; P = 0.95;
for i = 1:k-2
    if max(name{i,1}(1:5) ~= name{i+1,1}(1:5))
        if m == 1                % first interval
            nu = i-1;
            t = tinvc(P,nu);
            ad(m) = mean(nd(1:i,1));
            sd(m) = std(nd(1:i,1));
            ud(m) = t*sd(m)/sqrt(nu+1);
            clbd(m) = ad(m)-ud(m);
            cubd(m) = ad(m)+ud(m);
        else                    % middle intervals
            nu = i-(n+1)-1;
            t = tinvc(P,nu);
            ad(m) = mean(nd(n+1:i,1));
            sd(m) = std(nd(n+1:i,1));
            ud(m) = t*sd(m)/sqrt(nu+1);
            clbd(m) = ad(m)-ud(m);
            cubd(m) = ad(m)+ud(m);
        end
        n = i;
        m = m+1;
    end
end
                                % last interval

```

```

nu = i-(n+1)-1;           % degrees of freedom
t = tinvc(P,nu);          % corresponding t value
ad(m) = mean(nd(n+1:i,1)); % average diameter value
sd(m) = std(nd(n+1:i,1));  % st dev of diameter values
ud(m) = t*sd(m)/sqrt(nu+1); % uncertainty of diameter
values
clbd(m) = ad(m)-ud(m);     % confidence interval lower
bound
cubd(m) = ad(m)+ud(m);     % confidence interval upper
bound

% Round Statistics Results
for i = 1:m
    ad(i) = round(ad(i)*100)/100;
    ud(i) = round(ud(i)*10000)/10000;
end

% Manually Define Row Names
uname{1} = 'Mixture 1';
uname{2} = 'Mixture 2';
uname{3} = 'Acetone';
uname{4} = 'Ethanol';
uname{5} = 'Water';

%%%%%%%%%%%%%%%%%%%%%%%%%%%%%%%%%%%%%%%%%%%%%%%%%%%%%%%%%%%%%%%%%%%%%%%%
%%%%%%%%%%%%%%%%%%%%%%%%%%%%%%%%%%%%%%%%%%%%%%%%%%%%%%%%%%%%%%%%%%%%%%%%

% Output Table
Drop_Geo = table(rd,rA,rE,rC,'VariableNames',{'Diameter
(mm)'}...
    'Area
(mm^2)','Eccentricity','Circularity'},'RowNames',...
    name)

Diam_Stat = table(ad',ud', 'VariableNames',{'Average
Diameter (mm)'}...
    'Uncertainty (mm)'}, 'RowNames',uname)

```

```

%%%%%%%%%%%%%%%%%%%%%%%%%%%%%%%%%%%%%%%%%%%%%%%%%%%%%%%%%%%%%%%%%%%%%%%%
%%%%%%%%%%%%%%%%%%%%%%%%%%%%%%%%%%%%%%%%%%%%%%%%%%%%%%%%%%%%%%%%%%%%%%%%
% End Timer of Code
toc

```

Background Subtraction Code

```

%%%%%%%%%%%%%%%%%%%%%%%%%%%%%%%%%%%%%%%%%%%%%%%%%%%%%%%%%%%%%%%%%%%%%%%%
%%%%%%%%%%%%%%%%%%%%%%%%%%%%%%%%%%%%%%%%%%%%%%%%%%%%%%%%%%%%%%%%%%%%%%%%
% Clear Current Information
clearvars,close all,clc

%%%%%%%%%%%%%%%%%%%%%%%%%%%%%%%%%%%%%%%%%%%%%%%%%%%%%%%%%%%%%%%%%%%%%%%%
%%%%%%%%%%%%%%%%%%%%%%%%%%%%%%%%%%%%%%%%%%%%%%%%%%%%%%%%%%%%%%%%%%%%%%%%
% Read Data
tic

path = 'filepath_to_data';
                                % file path with data
subpath = genpath(path);       % all folders under
path
folders = split(subpath,';');  % first folder is path
folder and
                                % last folder is always
empty cell
nf = length(folders)-2;        % number of folders of
data
nsf = 5;                       % number of data files
in each folder
files = struct('name',cell(nsf,nf),'folder',cell(nsf,nf));
                                % memory allocation
j = 1;                         % counting variable
for i = 2:nf+1                 % skip path folder and
end before

```

```

                                % empty cell
    while isempty(files(1,j).name) == 0
                                % increment j until
empty cell is found
        j = j+1;
    end
    data = dir(strcat(folders{i,1},'\*.avi'));
                                % obtain file
information for all
                                % avi video files
    files(1,j).name = data(1).name; % file name
    files(1,j).folder = data(1).folder;
                                % folder directory and
name
    k = length(data);           % number of .avi files
in the folder
    for m = 2:k                 % loop through extra
.avi files
        files(m,j).name = data(m).name;
        files(m,j).folder = data(m).folder;
                                % cell array of file
information
    end
end

toc
%%%%%%%%%%%%%%%%%%%%%%%%%%%%%%%%%%%%%%%%%%%%%%%%%%%%%%%%%%%%%%%%%%%%%%%%%%%%%%
%%%%%%%%%%%%%%%%%%%%%%%%%%%%%%%%%%%%%%%%%%%%%%%%%%%%%%%%%%%%%%%%%%%%%%%%%%%%%%
% Basic Data Info
tic

n = 0;                          % number of files
for i = 1:nf                    % loop through folders
    for j = 1:nsf               % loop through files in
folders
        add = (0 == isempty(files(j,i).name));

```

```

        n = n+add;                                % total number of .avi
files
    end
end

toc
%%%%%%%%%%%%%%%%%%%%%%%%%%%%%%%%%%%%%%%%%%%%%%%%%%%%%%%%%%%%%%%%%%%%%%%%%%%%%%
%%%%%%%%%%%%%%%%%%%%%%%%%%%%%%%%%%%%%%%%%%%%%%%%%%%%%%%%%%%%%%%%%%%%%%%%%%%%%%
% Obtain Frames of Interest
tic

ef = zeros(nsf,nf);                                % end frame of interest
f = zeros(nsf,nf);                                % number of frames mem
allocate
mkdir 'Background_Subtracted'                    % create folder to
write new data
cd 'Background_Subtracted '                       % make that folder the
current folder
for i = 1:nf                                        % loop through all
files
    for j = 1:nsf                                    % loop through all sub-
files if any
        tic                                        % start timer for each
video process

        if 0 == isempty(files(j,i).name)
                                                    % skip the file if it
is empty
            FILENAME =
strcat(files(j,i).folder, '\', files(j,i).name);
                                                    % file name and dir of
files found
            V = VideoReader(FILENAME);
                                                    % read video data
            if V.VideoFormat ~= 'Grayscale'
                V = rgb2gray(V);    % convert video to

```

```

    grayscale
        end
        iF = read(V,1);           % initial frame of
video
        aIi = mean(mean(iF));    % average intensity of
background
                                   % assuming first frame
is background
        aI = aIi;               % reset average
intensity value
                                   % between loops
        BSV = Videowriter('BS' + " " +
files(j,i).name);
                                   % create video writing
object for
                                   % background subtracted
video
        open(BSV)               % open video writing
object
        rI = 0;                 % relative intensity
video cutoff
        while aI/aIi > rI       % loop through frames
of video until
                                   % the intensity ratio
is below rI
            ef(j,i) = ef(j,i)+1;
                                   % current frame of
comparison
            if V.NumFrames < ef(j,i)
                                   % if the end of the
video is reached
                ef(j,i) = ef(j,i)-1;
                                   % do not go over frame
total
                break           % exit while loop
        end

```

```

        cF = read(V,ef(j,i));
                                % current frame of
video
        aI = mean(mean(cF));% average intensity of
cF
        BSVD{j,i,ef(j,i)} =
uint8(double(cF)./double(iF)*aI);
                                % background subtracted
videos
                                % converted to double
to allow
                                % mathematical
operations, and
                                % back to uint8 to
write data
        writeVideo(BSV,BSVD{j,i,ef(j,i)})
                                % writes the new video
file frame
                                % by frame, hence the
loop
        end
        close(BSV)
                                % close the video
writing object
        toc
                                % end timer for each
video process
        end
    end
end
cd ..
                                % return to higher
directory
toc

```


BIBLIOGRAPHY

1. Liang, G., *Review of mass and momentum interactions during drop impact on a liquid film*. International Journal of Heat and Mass Transfer, 2016: p. 23.
2. Pack, M., et al., *Failure mechanisms of air entrainment in drop impact on lubricated surfaces*. Soft Matter, 2017. **13**(12): p. 2402-2409.
3. Kolinski, J.M., L. Mahadevan, and S.M. Rubinstein, *Drops can bounce from perfectly hydrophilic surfaces*. Europhysics Letters (EPL), 2014: p. 6.
4. Li, E.Q., et al., *Double Contact During Drop Impact on a Solid Under Reduced Air Pressure*. Physical Review Letters, 2017. **119**(21): p. 214502.
5. Worthington, A.M., III. *A second paper on the forms assumed by drops of liquids falling vertically on a horizontal plate*. 1877: p. 6.
6. Yarin, A.L., *DROP IMPACT DYNAMICS: Splashing, Spreading, Receding, Bouncing....* Annual Review of Fluid Mechanics, 2006. **38**(1): p. 159-192.
7. Avedisian, S.C.a.C.T., *On the collision of a droplet with a solid surface*. Proceeding of the Royal Society A, 1991: p. 29.
8. Driscoll, M.M., C.S. Stevens, and S.R. Nagel, *Thin film formation during splashing of viscous liquids*. Physical Review E, 2010. **82**(3): p. 036302.
9. Driscoll, M.M. and S.R. Nagel, *Ultrafast Interference Imaging of Air in Splashing Dynamics*. Physical Review Letters, 2011. **107**(15): p. 154502.
10. Mehdi-Nejad, V., J. Mostaghimi, and S. Chandra, *Air bubble entrapment under an impacting droplet*. Physics of Fluids, 2003. **15**(1): p. 173-183.
11. Thoroddsen, S.T., et al., *The air bubble entrapped under a drop impacting on a solid surface*. Journal of Fluid Mechanics, 2005. **545**(-1): p. 203.
12. Lee, J.S., et al., *How Does an Air Film Evolve into a Bubble During Drop Impact?* Physical Review Letters, 2012. **109**(20): p. 204501.

13. Duchemin, L. and C. Josserand, *Rarefied gas correction for the bubble entrapment singularity in drop impacts*. Comptes Rendus Mécanique, 2012. **340**(11-12): p. 797-803.
14. Fujimoto, H., H. Shiraishi, and N. Hatta, *Evolution of liquid/solid contact area of a drop impinging on a solid surface*. International Journal of Heat and Mass Transfer, 2000. **43**(9): p. 1673-1677.
15. Mandre, S., M. Mani, and M.P. Brenner, *Precursors to Splashing of Liquid Droplets on a Solid Surface*. Physical Review Letters, 2009. **102**(13): p. 134502.
16. Mani, M., S. Mandre, and M.P. Brenner, *Events before droplet splashing on a solid surface*. Journal of Fluid Mechanics, 2010. **647**: p. 163-185.
17. de Ruiter, J. and R. Lagraauw, *Wettability-independent bouncing on flat surfaces mediated by thin air films*. NATURE PHYSICS, 2015. **11**: p. 6.
18. Bouwhuis, W., et al., *Maximal Air Bubble Entrainment at Liquid-Drop Impact*. Physical Review Letters, 2012. **109**(26): p. 264501.
19. de Ruiter, J., et al., *Bouncing on thin air: how squeeze forces in the air film during non-wetting droplet bouncing lead to momentum transfer and dissipation*. Journal of Fluid Mechanics, 2015. **776**: p. 531-567.
20. de Ruiter, J., D. van den Ende, and F. Mugele, *Air cushioning in droplet impact. II. Experimental characterization of the air film evolution*. Physics of Fluids, 2015. **27**(1): p. 012105.
21. Klaseboer, E., R. Manica, and D.Y.C. Chan, *Universal Behavior of the Initial Stage of Drop Impact*. Physical Review Letters, 2014. **113**(19): p. 194501.
22. Kolinski, J.M., et al., *Skating on a Film of Air: Drops Impacting on a Surface*. Physical Review Letters, 2012. **108**(7): p. 074503.
23. Kolinski, J.M., L. Mahadevan, and S.M. Rubinstein, *Lift-Off Instability During the Impact of a Drop on a Solid Surface*. Physical Review Letters, 2014. **112**(13): p. 134501.
24. van der Veen, R.C.A., et al., *Direct measurements of air layer profiles under impacting droplets using high-speed color interferometry*. Physical Review E, 2012. **85**(2): p. 026315.

25. Li, E.Q. and S.T. Thoroddsen, *Time-resolved imaging of a compressible air disc under a drop impacting on a solid surface*. Journal of Fluid Mechanics, 2015. **780**: p. 636-648.
26. Langley, K., E.Q. Li, and S.T. Thoroddsen, *Impact of ultra-viscous drops: air-film gliding and extreme wetting*. Journal of Fluid Mechanics, 2017. **813**: p. 647-666.
27. Li, E.Q., I.U. Vakarelski, and S.T. Thoroddsen, *Probing the nano-scale: The first contact of an impacting drop*. Journal of Fluid Mechanics, 2015: p. 13.
28. Shirota, M., et al., *Measuring thin films using quantitative frustrated total internal reflection (FTIR)*. The European Physical Journal E, 2017. **40**(5): p. 54.